Title Page

Title: Elevated Lactate in Acute Myeloid Leukemia Bone Marrow Microenvironment Dysfunction, with a Dual Role of GPR81 in Macrophage Polarization and Leukemia Cell Growth

Authors and Affiliations:

Celia A. Soto[1,2,3], Maggie L. Lesch[2,4], Azmeer Sharipol[2,3,5], Amal Khan[2,3,4], Xenia L. Schafer[6], Michael W. Becker[2,7], Joshua C. Munger[4,6], Benjamin J. Frisch[1,2,3,5]

[1]Department of Pathology, University of Rochester School of Medicine, Rochester, NY, USA

[2]Wilmot Cancer Institute, University of Rochester Medical Center, Rochester, NY, USA

[3]Center for Musculoskeletal Research, University of Rochester Medical Center, Rochester, NY, USA

[4]Department of Microbiology and Immunology, University of Rochester School of Medicine, Rochester, NY, USA

[5]Department of Biomedical Engineering, University of Rochester School of Medicine, Rochester, NY, USA

[6]Department of Biochemistry and Biophysics, University of Rochester School of Medicine, Rochester, NY, USA

[7]Department of Medicine, University of Rochester School of Medicine, Rochester, NY, USA

Running Title:

Lactate-GPR81 Signaling in AML Progression

Keywords:

Acute Myeloid Leukemia (AML), bone marrow microenvironment, hematopoiesis, lactate, macrophages

Additional Information:

Financial support from the Wilmot Cancer Institute Research Development Funding Program Pilot Award to Dr. Frisch and Dr. Munger, and from a National Research Service Award (NRSA) Institutional Research Training Grant (T32) from the NIH to Celia Soto through the Rochester Musculoskeletal (ROCMSK) Training Program at the University of Rochester Center for Musculoskeletal Research (CMSR).

Corresponding Author:
Benjamin J. Frisch, Ph.D., University of Rochester Medical Center, School of Medicine and Dentistry. 601 Elmwood Avenue, Box 704, Rochester, NY, 14642. 1-(585)-275-5082, Benjamin_Frisch2@urmc.rochester.edu

Conflict of Interest Disclosure: There are no conflicts of interest to be disclosed by the authors.

Total Number of Figures and Tables: 6 main figures, 6 supplementary figures, 2 tables, and 2 supplementary tables, supplementary methods, and 2 supplementary methods tables.

Abstract

Interactions between acute myeloid leukemia (AML) and the hematopoietic bone marrow microenvironment (BMME) are critical to leukemia progression and chemoresistance. We measured elevated extracellular metabolites in the BMME of AML patients, including lactate. Lactate has been implicated in solid tumors for inducing suppressive tumor-associated macrophages, and correlates with poor prognosis. We describe a role of lactate in the polarization of leukemia-associated macrophages (LAMs), using a murine model of blast crisis chronic myelogenous leukemia (bcCML). Elevated lactate also diminished the function of hematopoietic progenitors and stromal support *in vitro*. Mice genetically lacking the lactate receptor GPR81 were used to demonstrate lactate-GPR81 signaling as a mechanism of both the polarization of LAMs and the direct support of leukemia cells. We report microenvironmental lactate as a critical driver of AML-induced BMME dysfunction and leukemic progression, thus identifying GPR81 as an exciting and novel therapeutic target for the treatment of this devastating disease.

Significance:

This research detects elevated metabolites in AML bone marrow and identifies GPR81-lactate signaling as a mechanism of leukemia progression. This preclinical data supports novel therapeutic strategies in the treatment of AML.

INTRODUCTION

Acute myeloid leukemia (AML) is within the top ten cancer subtypes with the most numerous deaths per year in the U.S. [SEER, NIH], with a ~90% mortality rate at five years past diagnosis in the most affected age group of 65+ (1). Cell-targeted chemotherapies initially reduce leukemic burden; however, there are various adverse effects on hematopoietic tissues, and relapse occurs in most patients (2, 3). AML patients are often poor candidates for more effective stem cell transplantation due to comorbidities (4). With approximately 20,000 new cases in the United States annually [SEER, NIH] and an increasing global incidence (5), there is a clear, unmet need for safe and effective treatments.

Current treatments for AML are often ineffective due, in part, to dysfunction of the bone marrow microenvironment (BMME). The BMME consists of all interactions among cells and extracellular molecules within the bone marrow (BM). AML is a heterogeneous hematologic malignancy initiated by genetic mutations in immature myeloid progenitor cells. Leukemic myeloid-like blasts undergo an uncontrolled proliferation (clonal hematopoiesis) and accumulate in the BM and other tissues (6). Secondary to BMME aberrations are cytopenia and eventual fatal infection, hemorrhage, or BM failure (7, 8). To date, the molecular mechanisms of the interactions between AML and the BMME in disease pathophysiology have not been fully explored.

Signaling within the BMME directs blood cell precursors to be produced from hematopoietic stem cells (HSCs) (9). When not circulating, HSCs reside at endosteal and perivascular areas within the BM termed HSC “niches” where they receive signals from specialized cells to remain quiescent, self-renew, or exit the niche to begin to differentiate into hematopoietic progenitors (10, 11). Multiple cell types have been implicated in the regulation of HSCs including specialized subsets of mesenchymal stromal cells (MSCs) (12-14), osteoblasts (OBs) (15-18), skeletal lineage cells (19), endothelial cells (20-22), macrophages (23), and T cells (24). Niche cells signal by cell-cell contact and secretion of numerous regulatory factors, including extracellular cytokines and inflammatory molecules (13, 25-31). Therefore, the BMME must maintain cellular and extracellular composition for hematopoietic homeostasis. BMME alterations can initiate or support leukemogenesis, and, reciprocally, leukemia results in an altered BMME (29, 32, 33); the consequence is diminished production of blood and immune cell populations. Furthermore, AML cells take refuge at the niche, leading to relapse when leukemia

stem cell (LSC) populations survive and repopulate after treatment (34, 35). Therefore, a thorough understanding of the microenvironment is needed to improve treatment.

Recent advances in the knowledge of the solid tumor microenvironment (TME) of multiple cancer types have revealed the complexities of cancer progression, leading to breakthrough therapeutic approaches such as immunotherapies. However, immunotherapies have not yet been effective in clearing LSC populations in AML (36). The TME has highly altered levels of extracellular metabolites and cytokines that render immune cells ineffective while supporting cancer cells (37-39). Thus far, the contribution of the extracellular metabolic landscape toward AML progression has not been well-defined. The altered extracellular metabolites in the TME often are attributed to the amplified metabolic drive of cancer cells and the small area between cells within the tumor architecture (40). In contrast, the BMME has a less compact tumor architecture, with ample vessel availability for nutrient and oxygen transfer throughout. Our research aimed to determine if similar metabolic microenvironmental mechanisms of cancer progression apply to leukemias.

A hallmark of cancer is the metabolic switch to constitutive aerobic glycolysis, known as “the Warburg effect” (41), and leukemia cells are dependent on this type of metabolism for survival (42). As a by-product of glycolysis, lactate is secreted to the extracellular microenvironment (43). Normally, lactate is converted back to pyruvate by lactate dehydrogenase (LDH) for further use of pyruvate as a metabolic substrate (44); however, 5-30-fold elevation of lactate levels have been reported in solid tumors (45) and this elevation correlates with poor prognosis (46). Lactate is imported/exported cellularly through monocarboxylate transporters (MCT)-1 and -4 and can signal through multiple pathways: as the extracellular ligand for the cell-surface G-protein-coupled hydroxycarboxylic acid receptor 1 (GPR81/HCAR1), and intracellularly as metabolic fuel or by activating transcription factor hypoxia-inducible factor-1 (HIF-1) (44, 47-49). These pathways primarily coordinate the axis between oxidative phosphorylation and glycolysis, and shifts in metabolism can influence cell phenotype, for example, the activation phenotype of macrophages (50). Lactate-GPR81 signaling was found to reprogram glucometabolism in breast cancer cells and directly contribute to the immune landscape in the TME (51). Downstream of GPR81 activation in cancer cells, pathways are upregulated for growth and survival, DNA repair proteins, chemoresistance (ex. ABCB1 transporter), and MCT1/4 expression (52-54). Moreover, GPR81-lactate signaling has

dual effects of inciting immune evasion by upregulating PD-L1 on cancer cells while dysregulating antigen presentation on immune cells (55, 56).

Furthermore, immunosuppressive tumor-associated macrophages (TAMs) correlate with poor prognosis in multiple cancer types, with lactate signaling implicated as a mechanism of polarization (57-61). In the BMME, macrophages are integral to the HSC niche during normal hematopoiesis and stress (62, 63), and they interact with MSCs to coordinate the circulation of HSCs (14). While recent studies show alternatively activated leukemia-associated macrophages (LAMs) and suggest their influence on AML progression (64, 65), little is known about the functions of LAMs and the mechanisms by which they are polarized to this phenotype. Therefore, we hypothesized that metabolite-related alterations to macrophages, MSCs, or OBs likely disrupt hematopoietic support, contributing to the pathologic loss of hematopoiesis observed in AML progression. We also aimed to determine if, similar to solid tumors, lactate contributes to both an alternative macrophage phenotype and direct support for malignant cells.

RESULTS

Extracellular Metabolite Levels are Elevated in Bone Marrow of AML Patients, Including Lactate

To profile the exometabolome of the AML bone marrow microenvironment (BMME), we performed metabolomics on extracellular fluid from bone marrow (BM) biopsies of AML patients at diagnosis, and healthy age- and sex-matched controls, by liquid chromatography coupled to mass spectrometry (LC-MS/MS) (**Fig. 1A**) (See patient and control metrics in **Table S1**). This revealed a global elevation of extracellular metabolites in the AML BMME (**Fig. 1B**), where **Table 1** lists the metabolites with significantly altered levels (**Supplementary Fig. 1A**). To study the consequences of elevated metabolites *in vivo*, we used a murine AML model of blast-crisis chronic myelogenous leukemia (bcCML), where gene translocation products common to myeloid leukemia (BCR-ABL) and (NUP98-HOXa9) are retrovirally inserted into hematopoietic stem and progenitor cells (HSPCs/LSKs) to create malignant myeloid progenitor cells, that, upon injection via tail vein, will engraft then accumulate rapidly in the BM, and irradiation is not necessary to precondition the BM (66). In this model, leukemic cells can be distinguished from nonleukemic myeloid lineage cells, by the use of the leukemic genes conjugated to green

Fig. 1)

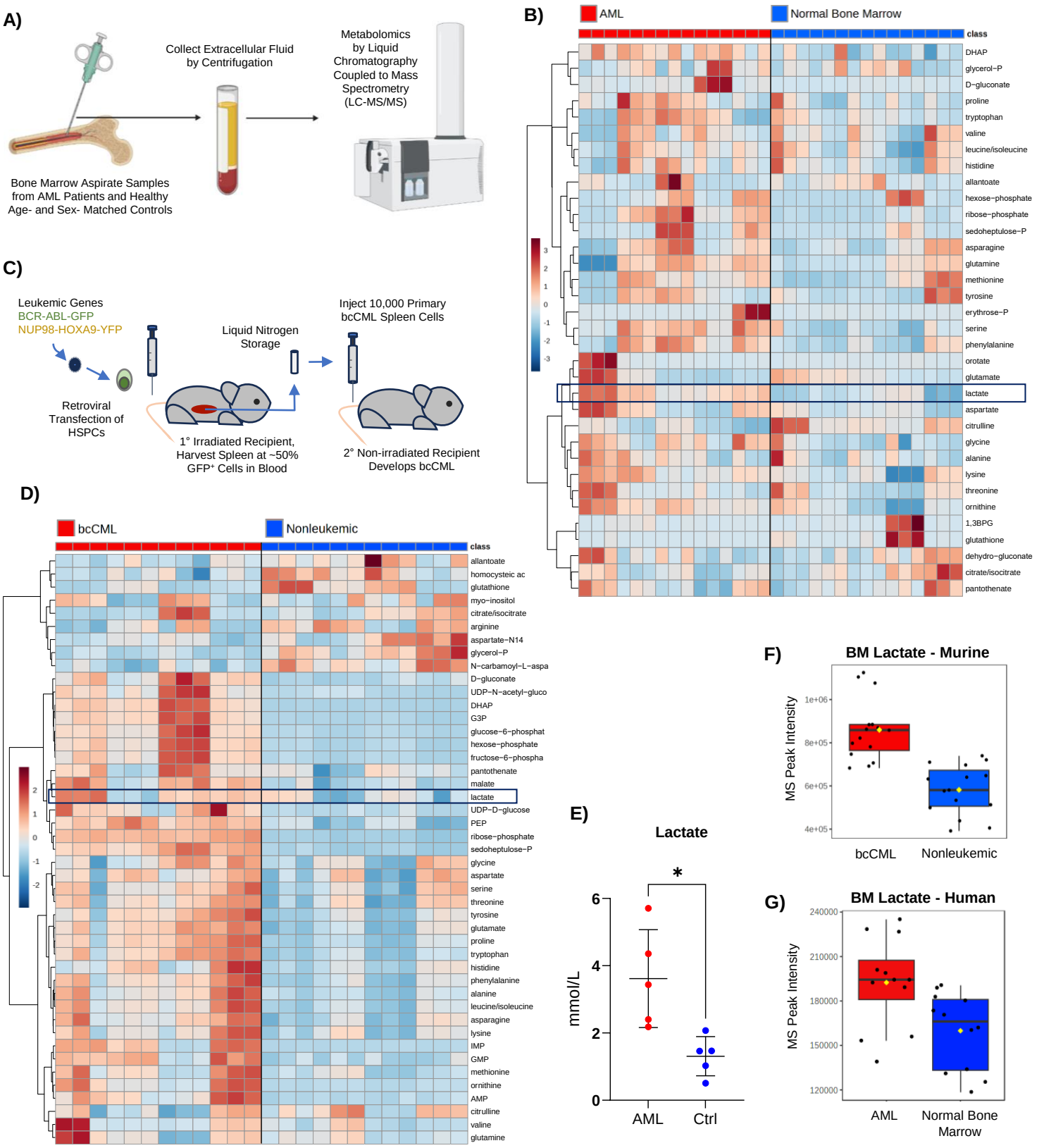

Fig. 1) Lactate is elevated in the bone marrow microenvironment (BMME) during acute myeloid leukemia (AML).

A, Graphical description of the process for metabolomic analysis of human AML vs. normal control BM extracellular fluid. **B,** Heatmap showing the relative abundance of detectable metabolites in human BM extracellular fluid of AML patients vs. controls (n = 5, in triplicates). **C,** Graphical depiction of the procedure for the generation of leukemic cells and initiation of bcCML, a murine AML model. **D,** Heatmap showing the relative abundance of detectable metabolites in murine bcCML vs. healthy BM extracellular fluid (n = 4, in triplicates). **E,** Absolute lactate concentration in AML and control human BM extracellular fluid (n = 5). **F** and **G,** Mass spectrometry (MS) peak intensity of lactate in murine (**F**) and human (**G**) BM extracellular fluid. Significance levels determined by unpaired t test for **E** is indicated as *, $P < 0.05$. Error bar indicates mean ± standard deviation (SD).

fluorescent protein (GFP) and yellow fluorescent protein (YFP) (**Fig. 1C**). The BMME at late-stage bcCML (>50% leukemia cells in BM) also presented with elevated extracellular metabolites (**Fig. 1D**), where **Table S2** lists the compounds with the most significantly altered levels (identified in **Supplementary Fig. 1B**). The most highly altered metabolite in human AML was lactate, with an extracellular lactate concentration approximately three times higher (**Fig. 1E**). The relative increase of lactate in the bcCML model was comparable to the human BMME (**Fig. 1F** and **1G**), justifying the use of this model for our further studies on microenvironmental lactate in AML pathology.

Table 1

Compound	t Stat	p Value	-log10(p)	FDR
lactate	5.86	2.66E-06	5.58	9.04E-05
serine	5.19	1.63E-05	4.79	0.00028
ribose-phosphate	4.37	0.00015	3.82	0.0016
citrulline	-4.29	0.00019	3.72	0.0016
DHAP	4.13	0.00029	3.54	0.0020
ornithine	3.84	0.00064	3.19	0.0037
phenylalanine	3.57	0.0013	2.88	0.0065
lysine	3.01	0.0054	2.26	0.023
glycine	2.88	0.0074	2.13	0.028

Table 1: Altered Extracellular Metabolites in Human AML Bone Marrow

Leukemia-Associated Macrophages are Alternatively Activated to a CD206^{hi}, Suppressive Phenotype

We asked if elevated lactate has a role in the activation/polarization of local macrophages to a pro-tumoral phenotype, as reported in solid tumors (57, 58, 60). First, we determined whether macrophages in the bcCML BM are alternatively activated. A survey of well-described activation markers [CD38 and major histocompatibility complex class II (MHCII) = classic, pro-inflammatory (67, 68); macrophage mannose receptor (CD206) and early growth response protein 2 (EGR2) = alternative, suppressive/resolution-phase (69, 70)] was performed on BM macrophages (Ly-6C$^-$, Ly-6G$^-$, CD45$^+$, F4-80$^+$) of bcCML mice (leukemia-associated macrophages (LAMs)) and non-leukemic (NL) controls (**Fig. 2A**) (See **Supplementary**

Fig. 2)

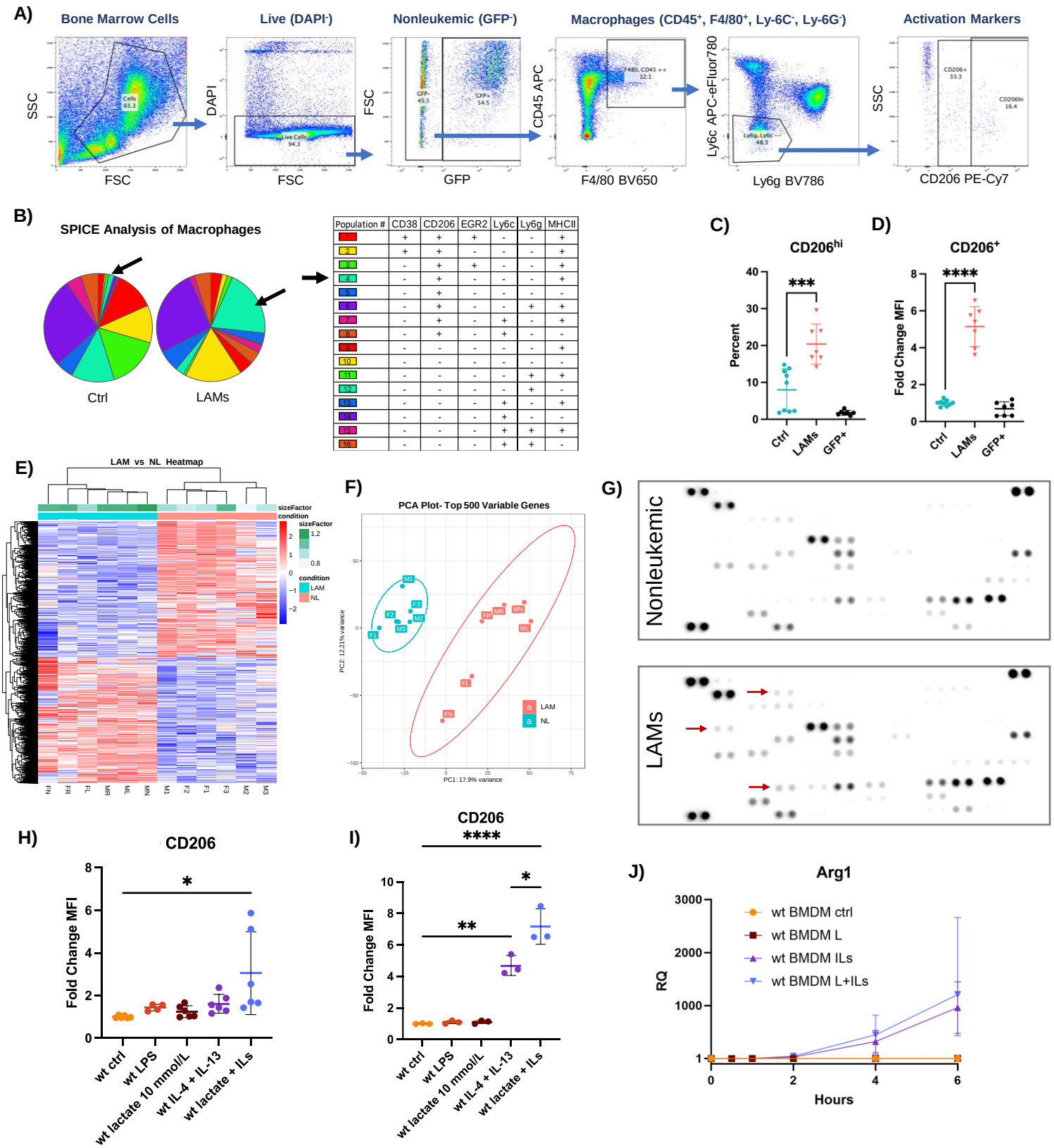

Population #	CD38	CD206	EGR2	Ly6c	Ly6g	MHCII
1	+	+	+	-	-	+
2	+	+	-	-	-	+
3	-	+	+	-	-	+
4	-	+	-	-	-	+
5	-	+	-	-	-	-
6	-	+	-	-	+	+
7	-	+	-	+	-	+
8	-	+	-	+	-	-
9	-	-	-	-	-	+
10	-	-	-	-	-	-
11	-	-	-	-	+	+
12	-	-	-	-	+	-
13	-	-	-	+	-	+
14	-	-	-	+	-	-
15	-	-	-	+	+	+
16	-	-	-	+	+	-

Fig. 2) Lactate contributes to the polarization of leukemia-associated macrophage (LAMs) to an alternatively activated phenotype. **A,** Gating scheme for flow cytometric analysis of murine BM macrophages. **B,** Simplified Presentation of Incredibly Complex Evaluations (SPICE) analysis of LAM subpopulations from late-stage bcCML (55-70% GFP$^+$ cells in BM) (n = 5), red arrows indicate populations lost and black arrow indicate populations enriched in disease. **C** and **D,** Frequency of CD206^{hi} (**C**) and mean fluorescence intensity (MFI) of CD206 on CD206$^+$ (**D**) non-leukemic control macrophages (Ctrl), leukemia-associated macrophages (LAMs), or leukemic (GFP$^+$) macrophages (n = 7). **E-F,** Bulk RNA sequencing of LAMs vs. macrophages from nonleukemic (NL) controls: heatmap of differentially expressed genes (**E**) and principal component analysis (PCA) of the top 500 variable genes (**F**). **G,** Cytokine profiling by ELISA of cell culture supernatant from NL macrophages or LAMs cocultured on a BM stromal monolayer (n = 2), representative example, arrows shown indicating a qualitative difference. **H** and **I,** Bone marrow-derived macrophage (BMDM) expression of CD206, polarized *in vitro* by treatment with 10 mmol/L lactate, lipopolysaccharide (LPS) as proinflammatory stimuli, and/or IL-4 and IL-13 as suppressive stimuli, in serum-free media for 12 hours (**H**) (n = 6) or 1 week (**I**) (n = 3). **J,** Range of relative quantification (RQ) of Arginase 1 (*Arg1*) transcripts in BMDMs polarized by lactate (L) and/or IL-4 and -13 (ILs), measured by RT-qPCR (n = 3, in duplicates). Significance levels determined by one-way ANOVA for **C, D, H,** and **I** are indicated as: *, $P < 0.05$; **, $P < 0.01$; ***, $P < 0.001$; ****, $P < 0.0001$. Error bar indicates mean ± SD.

Methods Table SM2 for markers and gating strategies). The software "Simplified Presentation of Incredibly Complex Evaluations" (SPICE 6.1) (NIH) was used to identify an increased subset of LAMs that overexpressed both CD206 and MHCII compared to NL macrophages (**Fig. 2B**). When assessing these markers globally on LAMs, we observed an increase in the frequency of $CD206^{hi}$ macrophages (**Fig. 2C**) and expression level on the $CD206^{+}$ macrophages (**Fig. 2D**); this was unique to non-leukemia-derived (GFP^{-}) macrophages and was elevated throughout the disease course (**Supplementary Fig. 2A**). This suggests CD206 as a potential marker to distinguish LAMs from myeloid leukemia cells in humans, of which there is not currently a good marker for. The global frequency of MHCII was generally lower in LAMs, and CD38 and EGR2 were unchanged (**Supplementary Fig. 2B-D**). Splenic macrophages had a slightly higher frequency of $CD206^{+}$ in bcCML, though the expression level on $CD206^{+}$ macrophages and the frequency of $CD206^{hi}$ macrophages were unchanged (**Supplementary Fig. 2E-I**). The increase in CD206 expression was detectable on BM LAMs by an early-stage disease (7-10% leukemic cells in the BM) (**Supplementary Fig. 2J** and **2K**).

To examine the functional phenotype of LAMs, transcriptional profiling was performed by bulk RNA sequencing (RNAseq) of BM macrophages sorted from bcCML (LAMs) or NL controls. The LAM transcriptome was distinctly different from NL macrophages (**Fig. 2E** and **2F**, and **Supplementary Fig. 2L**). The top significantly downregulated pathways identified included neutrophil interactions and cell cycle control (**Supplementary Fig. 2M**), while the top upregulated pathways included interactions with immune and hematopoietic cells (**Supplementary Fig. 2N**). This data indicates that LAMs are alternatively activated and may contribute to the immune-privileged and dysregulated hematopoietic BMME observed in AML. Proteome profiling detected several cytokines expressed by LAMs *in vitro* that were not secreted by NL macrophages (**Fig. 2G** and **Table 2**). These cytokines have previously been implicated in solid tumors as promoting tumor growth and metastasis (CXCL5, MMP3, proprotein convertase 9) (71-73), regulating hematopoietic stem cell (HSC) development and homing/mobilization (CXCL12)(74), and inducing a suppressive immune environment in the tumor (CXCL10, CCL6) (75, 76), further suggesting a role of LAMs in the regulation of the BMME to promote leukemic progression and suppress immune responses.

To isolate the contribution of lactate to the LAM phenotype, we treated bone marrow-derived macrophages (BMDMs) *in vitro* with physiologically relevant levels of lactate: BM

extracellular lactate concentrations are likely higher *in vivo* than the measured concentrations of ~2-5 mmol/L because AML patient BM biopsy samples are unavoidably diluted by some peripheral blood upon collection. Also, we postulate that areas exist near AML cell-dense pockets that are higher in lactate concentration, as the BM is known to be spatially heterogeneous for concentrations of similar molecules, and pH (77). Therefore, 5-15 mmol/L of lactate was added for experiment treatments. As positive controls, we used lipopolysaccharide (LPS) as proinflammatory stimuli (67), or interleukins (IL)-4 and -13 (IL-4, IL-13), well-described Th2 cytokines produced in the resolution of inflammation regularly used as stimuli for alternative macrophage activation (78-80). We observed an additive effect of polarization to a $CD206^{hi}$ phenotype when lactate was combined with IL-4 and IL-13 (**Fig. 2H** and **2I**). This indicates that lactate promotes polarization when some stimuli are present. The phenotype reversed after the removal of stimuli for 48 hours (**Supplementary Fig. 2O** and **2P**), indicating that the activation state is reversible. To assay for the function of $CD206^{hi}$ lactate-polarized BMDMs, we measured transcript levels of Arginase 1 (Arg1): an enzyme involved in depleting L-arginase, the substrate of inducible nitric oxide synthase (iNOS/Nos2), which mediates the cytotoxic production of nitric oxide by classically-activated macrophages (69, 81). Polarized BMDMs displayed increased *Arg1* transcripts (**Fig. 2J**), while *iNOS* transcripts were not elevated (**Supplementary Fig. 2Q**). These findings taken together suggest that macrophages in AML are likely suppressive, and that excess lactate sensitizes macrophages to become alternatively activated.

Table 2

Cytokine	Reported Functions
CXCL10/IP-10	Immunosuppressive Tumor Microenvironment
LIX (CXCL5)	Tumor Growth and Metastasis
CCL12 (MCP-5)	HSC Regulation and Homing
CCL6/C10 (MRP-1)	Immunosuppressive Tumor Microenvironment
MMP3	Tumor Growth and Metastasis
Proprotein Convertase 9	Tumor Growth and Metastasis

Table 2: Cytokines Upregulated in LAM Cocultures and Reported Functions in the BM or Cancer Progression

Elevated Lactate Negatively Regulates the Hematopoietic Bone Marrow Microenvironment

Within the unique cancer microenvironment of the bone marrow in AML, we must consider how excess lactate may affect hematopoiesis. As we have previously reported (82), the murine model of bcCML presented *in vivo* with an increase in the percentage of phenotypic hematopoietic stem and progenitor cells (HSPCs), also known as LSK cells, and multipotent progenitors (MPP): megakaryocyte-biased MPP2, myeloid-biased MPP3, and lymphoid-primed MPP4 (**Supplementary Fig. 3A-F,** see **Supplementary Methods Table SM2** for markers and gating strategies). Also as previously reported, MSCs were expanded within the leukemic bone (29), a key cell type for the maintenance of HSPCs; this was nonspecific to MSC subsets known to be important to HSC adhesion and self-renewal at the niche: PDGFRa/CD51 (PααV) or PDGFRa^{+}Sca-1^{+} (PαS) MSCs (**Supplementary Fig. 3G-I**) (83-85). Still, mature blood cell populations are lost by late-stage bcCML (82), showing a dysfunction in progenitor cell maintenance and/or differentiation.

To determine if lactate reduces the hematopoietic potential of HSPCs, colony-forming unit cell (CFU-C) assays [39, 40] were performed: HSPCs/LSKs from healthy mice were cocultured *in vitro* with a stromal monolayer and added “LSK” cytokines to promote the maintenance of stemness, and were treated experimentally. They are then passaged to methylcellulose-based MethoCult media (StemCell Technologies M3434) where they will grow as colonies (CFU-Cs) if they retain hematopoietic potential. The stromal monolayer is grown from the adherent cells from whole BM, and is composed of both a small percentage of MSCs (>1%, like the percentage seen in the bone *in vivo*), and macrophages (**Supplementary Fig. 3J** and **3K**). As we have previously reported that aged macrophages can alter the colony-forming potential of HSPCs (85), we tested the addition of LAMs to the cocultures compared to macrophages from NL mice (**Fig. 3A**). The HSPCs showed reduced CFU-Cs when cocultured with LAMs (**Fig. 3B**), suggesting a difference in hematopoietic maintenance signals. To determine if lactate has direct effects on HSPCs, CFU-C assays were performed on HSPCs alone (without a stromal monolayer). When treated with 10-15 mmol/L of lactate, HSPCs lost colony-forming potential after 48 or 72 hours (**Fig. 3C** and **3D**). We asked if stromal cells could maintain HSPCs in the presence of lactate, CFU-C assays with lactate treatment were repeated on cocultures of HSPCs with a stromal monolayer (**Fig. 3E**). However, cocultures treated with

Fig. 3)

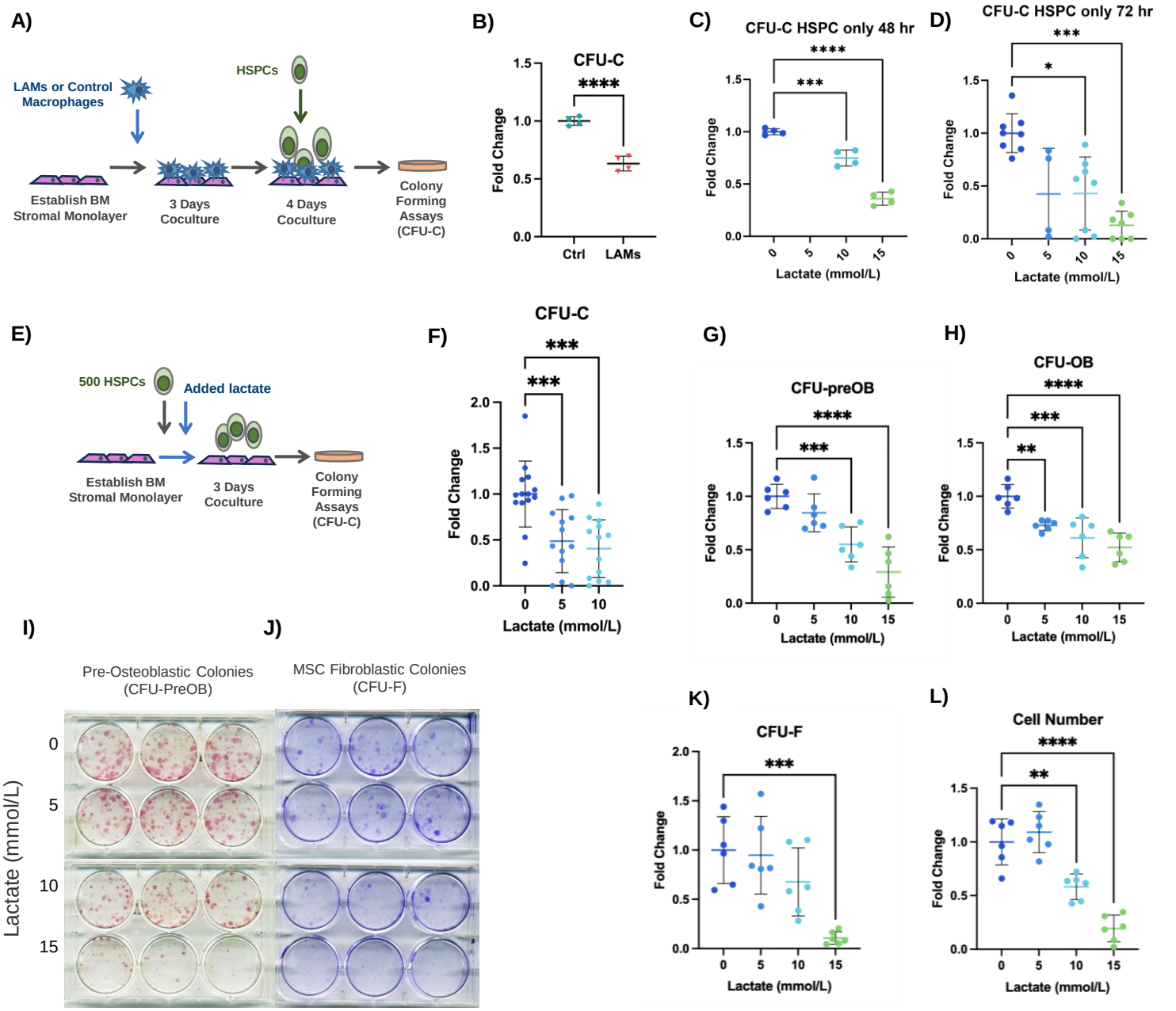

Fig. 3) Lactate drives loss of hematopoietic stem and progenitor cell (HSPC) function and support. **A,** Experimental procedure to assay for HSPC hematopoietic colony-forming potential, by colony-forming unit cell (CFU-C) assays: Murine HSPCs/LSKs are cocultured with a BM stromal monolayer and 60,000 added macrophages. **B,** CFU-Cs after coculture with LAMs or nonleukemic control (Ctrl) macrophages (n = 4). **C-D,** CFU-C of HSPCs alone, with or without added lactate for 48 hours (**C**) (n = 4) or 72 hours (n = 4-8) (**D**). **E-F,** CFU-C assays of HSPCs and stromal monolayer cocultures for 72 hours with or without added lactate: Experimental procedure (**E**), CFU-Cs relative to the 0 mmol/L lactate control group (**F**) (n = 12-14). **G-I,** BM MSC differentiation to osteoblasts (OBs) with or without lactate treatment: relative area of colony-forming unit pre-osteoblastic (CFU-preOB) colonies visualized with alkaline phosphatase staining at day 14 (**G**) (n = 6), relative area of calcium deposition measured by silver nitrate staining at day 28 (**H**) (n = 6), representative image of Pre-OB colonies (**I**). **J-L,** Lactate treatment of MSCs grown in a non-differentiation culture media: representative image of colony-forming unit fibroblast (CFU-F) (**J**) and relative colonies on day 10 (**K**) (n = 6), relative cell number of whole BM MSCs by day 14 (**L**) (n = 6). Significance levels determined by unpaired t test for **B** and by one-way ANOVA for **C-D**, **F-H**, and **K-L** are indicated as: *, $P < 0.05$; **, $P < 0.01$; ***, $P < 0.001$; ****, $P < 0.0001$. Error bar indicates mean ± SD.

lactate for 72 hours also showed reduced CFU-Cs (**Fig. 3F**), suggesting that stromal cells do not protect HSPCs from elevated lactate.

Next, we asked how excess lactate alters key stromal HSC niche cell types: MSCs and their bone-forming progeny, osteoblasts (OBs). Stromal cultures that were differentiated to OBs in the presence of increased lactate produced fewer pre-OB and OB colonies (**Fig. 3G-I**). This is consistent with a loss of functional OBs and bone volume that we have previously reported as a pathophysiology of AML [38]. Without differentiation, lactate also reduced MSC colony-forming ability to fibroblasts (CFU-F), a measure of MSC self-renewal potential, [36, 37] and decreased cell number after two weeks in culture (**Fig. 3J-L**). These results highlight multiple damaging effects of elevated lactate on critical components of hematopoiesis in the BM.

Lactate Signaling through GPR81 Contributes to the Suppressive Phenotype of Leukemia-Associated Macrophages

Lactate signals through multiple cellular pathways, therefore, we assessed which of these pathways result in the observed lactate-mediated AML pathologies. To study this *in vivo*, we considered the tools available: Genetic knockout of MCT1 is embryonically lethal (86), and while MCT4 knockout mice are viable (87), MCT1 would be present which has a higher affinity for lactate (88). However, mice genetically lacking the lactate receptor GPR81 (*Gpr81*$^{-/-}$ or GPR81KO) grow to healthy adulthood, produce blood cells at a normal ratio (**Supplementary Fig. 4A-F**), have a similar weight and BM cellular density as wt mice (**Supplementary Fig. 4G-J**), and GPR81 has been implicated in regulation of the cancer microenvironment in solid tumors. Therefore, we used GPR81KO mice to investigate the role of lactate-GPR81 signaling. First, wild type (wt) bcCML was initiated in GPR81KO mice to eliminate GPR81 signaling from all non-leukemic BM cells (**Fig. 4A**). The metabolomics of the BM extracellular fluid presented with elevated metabolites at similar levels to bcCML in wt mice (**Supplementary Fig. 4K**), which confirmed that this may be useful to study GPR81 signaling in the BMME during bcCML.

We reinvestigated the polarization of LAMs observed during bcCML when initiated in the *Gpr81*$^{-/-}$ BMME. The increased frequency of macrophages observed in bcCML was partially reversed in GPR81KO mice (**Fig. 4B**). The LAMs in the GPR81KO BMME expressed lower CD206 levels, nearer to macrophages of healthy NL control mice (**Fig. 4C** and **4D**), and the frequency of MHCII^{+} macrophages was higher (**Fig. 4E**). Other polarization markers were

Fig. 4)

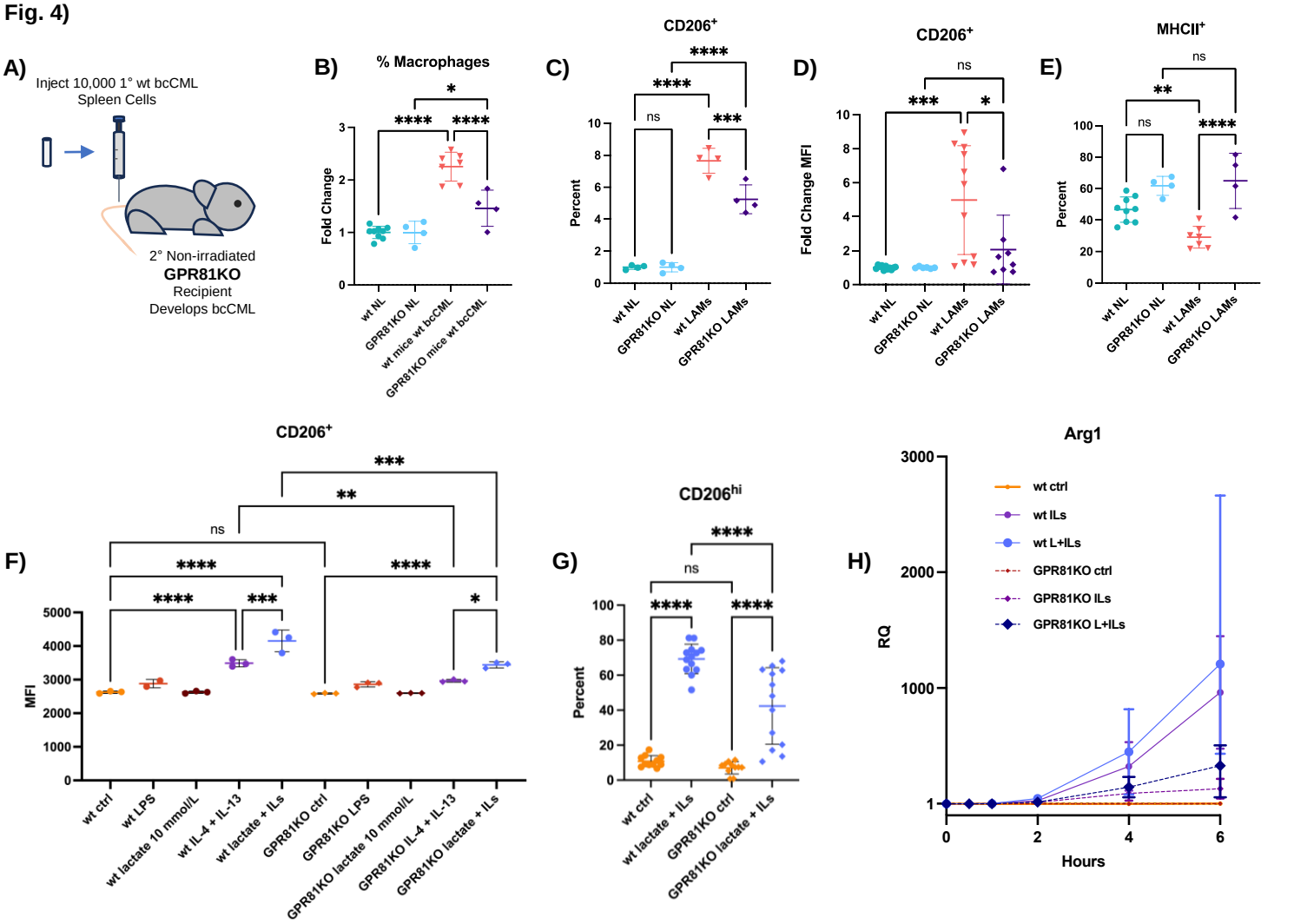

Fig. 4) GPR81 drives leukemia-associated macrophage (LAM) polarization.
A, Graphical depiction of the procedure for the initiation of wt bcCML in a *Gpr81*$^{-/-}$ BMME **B,** Frequency of macrophages, out of live non-leukemic (GFP^{-}) cells, from the BM of wt bcCML initiated in wt or *Gpr81*$^{-/-}$ (GPR81KO) mice, relative to nonleukemic (NL) controls of the same genetic background (n = 4-7). **C-E,** Marker expression on BM LAMs of wt bcCML initiated in wt or *Gpr81*$^{-/-}$ (GPR81KO) mice, or NL controls: Frequency of CD206^{+} macrophages in the BM (**C**), expression of CD206 on CD206^{+} BM macrophages relative to relative to NL controls of the same genetic background (**D**), frequency of MHCII^{+} BM macrophages (**E**) (n = 4-11). **F,** MFI of CD206 on CD206^{+} wt or *Gpr81*$^{-/-}$ BMDMs polarized by LPS, IL-4 and -13 (ILs), and/or 10 mmol/L lactate (n = 3). **G,** Frequency of CD206^{hi} wt or GPR81$^{-/-}$ BMDMs with or without polarization by ILs and lactate. **H,** Range of relative quantification (RQ) of *Arg1* expression by wt or GPR81KO BMDMs polarized by IL-4 and -13 (ILs) with or without lactate, measured by RT-qPCR (n = 3, in duplicates). Significance levels determined by one-way ANOVA for **B-G** are indicated as: ns, not significant; *, $P < 0.05$; **, $P < 0.01$; ***, $P < 0.001$; ****, $P < 0.0001$. Error bar indicates mean ± SD.

increased or unchanged (**Supplementary Fig. 4L-P**). The GPR81KO mice displayed a similar leukemic burden in the BM by the time of late-stage disease in wt mice, however, there was a significant decrease in the frequency of leukemia cells in the peripheral blood and spleen (**Supplementary Fig. 4Q-S**); this indicates a decrease in disease progression and/or a reduction of peripheralization of leukemia cells.

Assays for BMDM polarization *in vitro* confirmed the contribution of GPR81 signaling as a mechanism of LAM polarization; while they can be partially polarized, *Gpr81*$^{-/-}$ BMDMs did not upregulate CD206 as highly as wt BMDMs (**Fig. 4F** and **4G**) and had a reduced range of *Arg1* expression (**Fig. 4H**). To assay an additional signaling mechanism of lactate, we used syrosingopine as a dual inhibitor of MCT1/4 and observed a contribution of MCTs to polarization (**Supplementary Fig. 4T-V**), showing that other cell-internal signaling mechanisms of lactate also promote the alternative activation phenotype. Next, we checked expression levels of lactate signaling-related receptors in response to lactate treatment. When wt BMDMs were polarized, we observed an upregulation of *Mct1* mRNA expression (**Supplementary Fig. 4W** and **4X**), while there was not a significant increase in transcription of *Gpr81*, or *Mct4* (**Supplementary Fig. 4Y** and **4Z**). However, we did not observe significant transcriptional changes in the expression of *Gpr81*, *Mct1*, *Mct4*, or *iNOS* upon the polarization of GPR81KO BMDMs compared to wt BMDMs (**Supplementary Fig. 4AA**). Therefore, this suggests that, in macrophages, GPR81 sensing of lactate induces upregulation of MCT1 for lactate import/export.

GPR81-Lactate Signaling Has Modest Effects on the Hematopoietic BMME

Next, we investigated which hematopoietic populations are impacted by GPR81 signaling. The frequencies of hematopoietic progenitor, MSC, osteoblastic cell, and mature blood cell populations were generally unchanged when bcCML was initiated in GPR81KO mice compared to wt (**Fig. 5 A-I** and **Supplementary Fig. 5A**). This data, together with the fact that nonleukemic, adult *Gpr81*$^{-/-}$ mice have appropriate ratios of mature blood cells, suggests that GPR81 may be largely dispensable to hematopoiesis.

We assayed whether GPR81 signaling results in the observed lactate-mediated changes to the colony-forming potential of HSPCs and MSCs. *Gpr81*$^{-/-}$ HSPCs showed a trend towards a reversal of CFU-C loss at 5-10 mmol/L lactate with or without a stromal monolayer, but

Fig. 5)

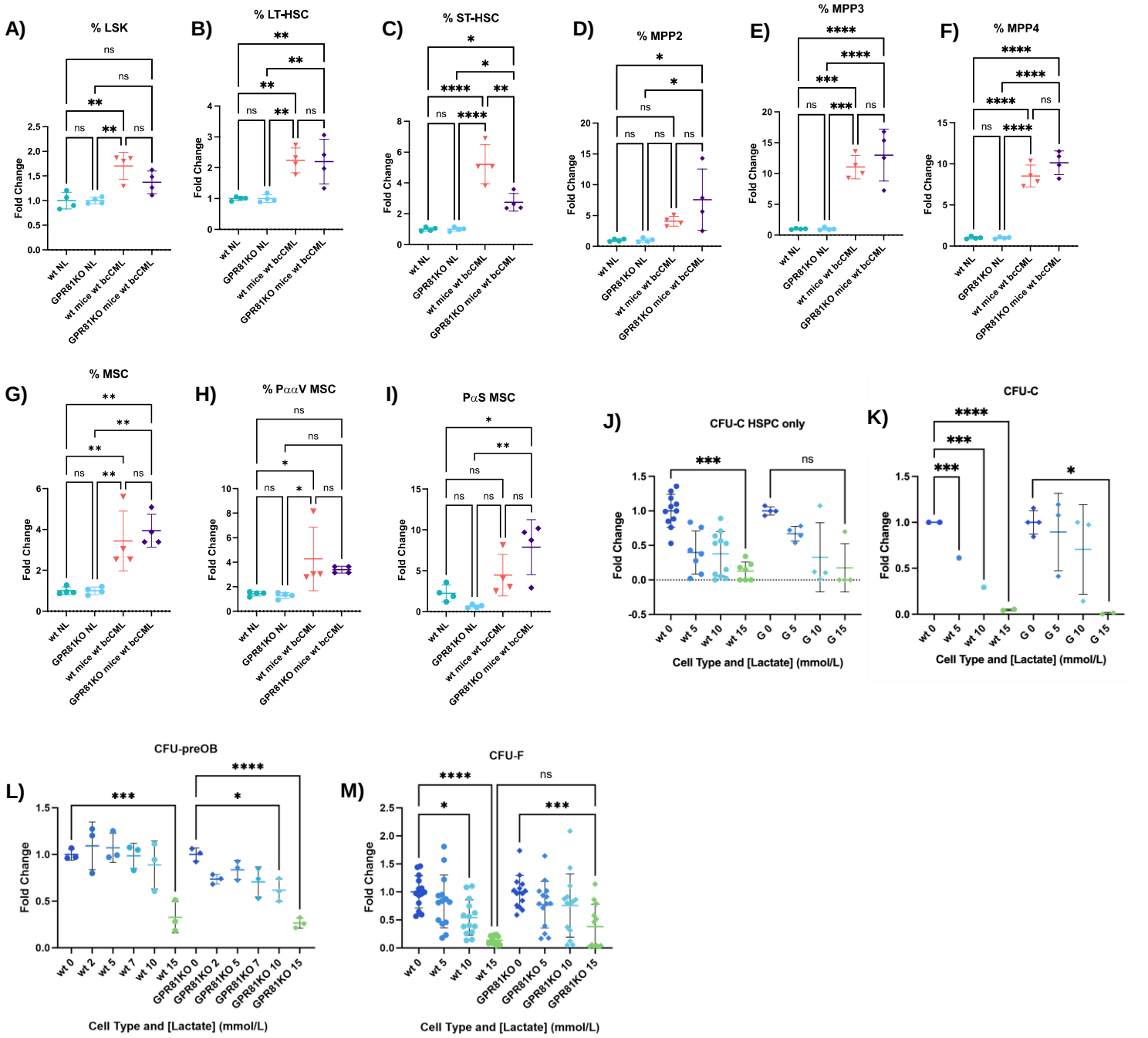

Fig. 5) GPR81 signaling partially regulates HSPC function.

A-F, Hematopoietic progenitors' frequency in the BM of wt bcCML initiated in wt or GPR81KO mice, relative to the nonleukemic (NL) control of the same genetic background: hematopoietic stem and progenitor cells (HSPCs/LSK) (**A**), long-term hematopoietic stem cell (HSC) (**B**), short-term HSC (**C**), multipotent progenitor (MPP) subsets MPP2 (**D**) MPP3 (**E**) and MPP4 (**F**) (n = 4). **G-I,** Mesenchymal stem cell (MSC) populations in bone: MSCs (**G**), PααV MSCs (**H**), and PαS MSCs (**I**) (n = 4). **J-K,** CFU-Cs of wt or *Gpr81*$^{-/-}$ (G^-) lactate-treated HSPCs alone (**J**) or with a stromal monolayer (**K**), relative to 0 mmol/L lactate (n = 4-8). **L-M,** CFU-preOB (**L**) and CFU-F (**M**) of wt or *Gpr81*$^{-/-}$ MSCs with lactate treatment, relative to the 0 mmol/L lactate control of the same genetic background. Significance levels determined by one-way ANOVA for all are indicated as: ns, not significant; *, $P < 0.05$; **, $P < 0.01$; ***, $P < 0.001$; ****, $P < 0.0001$. Error bar indicates mean ± SD.

potentiality still was lost by 15 mmol/L (**Fig. 5J** and **5K**). Also, lactate-treated *Gpr81*$^{-/-}$ MSCs still displayed a loss of pre-OBs and fibroblastic colonies (**Fig. 5L** and **5M**). To note, we observed a sex-dependent difference in CFU-F, where only MSCs from females were impacted by lactate at 5-10 mmol/L (**Supplementary Fig. 5B** and **5C**). We then tested whether MCT1/4 signaling is responsible for the losses at 15 mmol/L. First, treatment with syrosingopine at the 5 µM dose, used for the macrophage polarization experiments, was lethal to the MSCs. Syrosingopine treatments of 1 µM were not lethal, and caused a slight increase in CFU-F (**Supplemental Fig. 5D**). This demonstrates that MCT signaling is critical to MSC function; however, we note that MCT inhibitors, if used therapeutically, may have effects on crucial MSC populations at lower concentrations than to other cell types.

We assayed mRNA transcription levels of G*pr81* and *Mct1/4* by MSCs in response to lactate treatment when GPR81 signaling is not present. *Gpr81*$^{-/-}$ MSCs had a lower upregulation of *Mct4* than wt MSCs, while *Mct1* and *Gpr81* expression were similar to wt (**Supplementary Fig. 5E-G**). Therefore, in MSCs, GPR81 may act as a lactate-sensor to regulate MCT-mediated import/export of lactate; we hypothesize that this method of regulating intracellular lactate concentration thereby influences the metabolic pathway primarily used by the cell (namely, oxidative phosphorylation or glycolysis), which are known to influence the osteoblastic differentiation fate of MSCs (89). Altogether, these data show that GPR81 signaling has a modest impact on hematopoietic cell types and MSCs, therefore, it may be possible to therapeutically target lactate signaling in the BMME through this receptor with minimal consequences on hematopoiesis; However, this will not protect the colony-forming potential of HSPCs and MSCs from high lactate concentrations in bone.

Lactate-GPR81 Signaling Drives Leukemia Cell Growth and Repopulation

We hypothesized that BMME lactate also directly affects AML cells, as other cancer types have found GPR81 signaling to promote growth, chemoresistance, and metastasis (52-54, 56). To determine if lactate enhances leukemia cell growth, *Gpr81*$^{-/-}$ bcCML cells were generated; these were then used to initiate disease either in wt mice, so that GPR81 signaling remains in BMME cells, or in GPR81KO mice (double-knockout (DKO)) where GPR81 signaling is not present both on leukemic cells or in the BMME (**Fig. 6A**). When GPR81KO bcCML cells were used, the leukemic burden was then largely reduced in the BM, peripheral blood, and spleen of by the

Fig. 6)

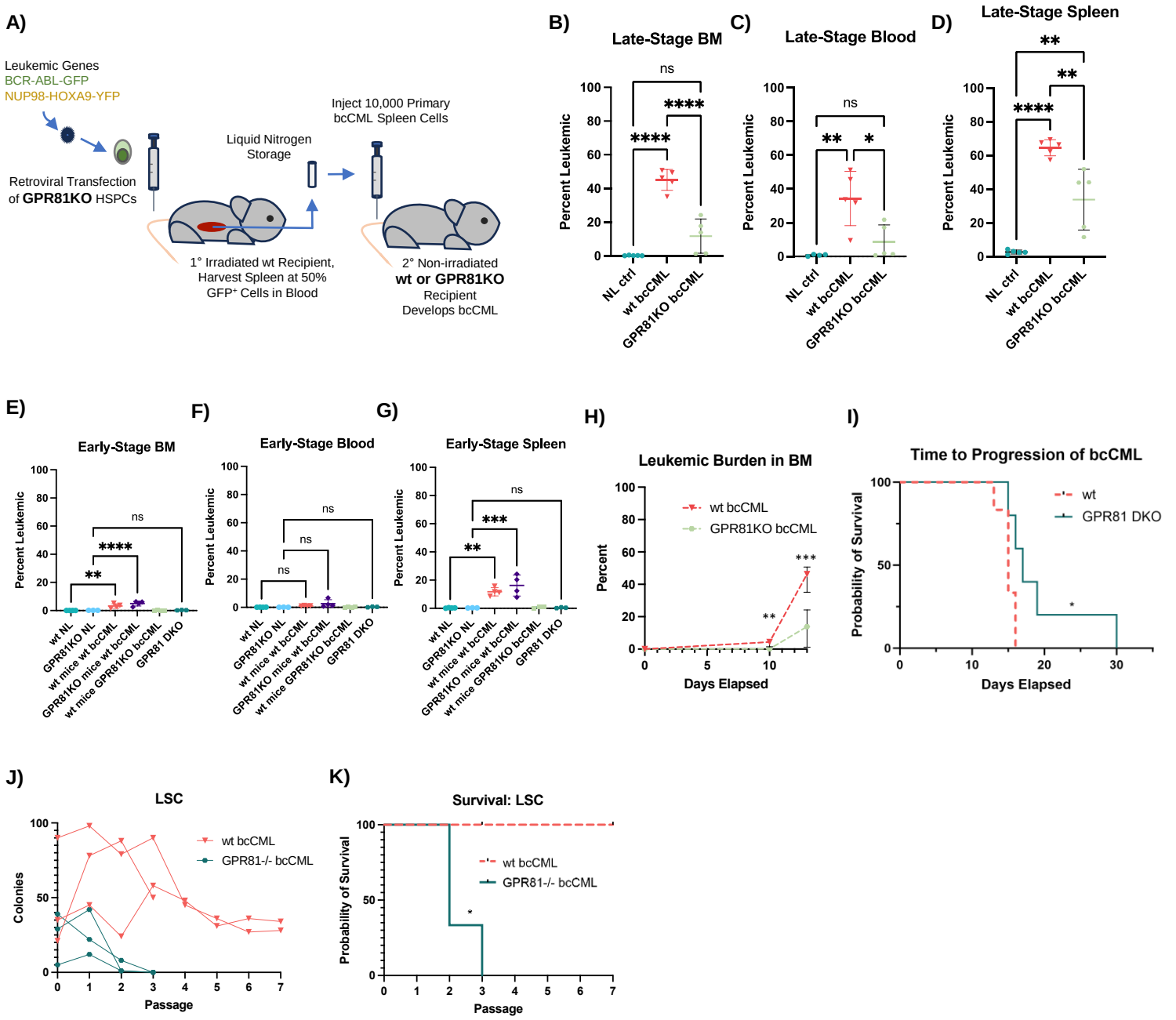

Fig. 6) GPR81 signaling is a driver of leukemia cell growth and leukemia stem cell (LSC) self-renewal. **A,** Graphical depiction of the procedure for the initiation of *Gpr81*$^{-/-}$ (GPR81KO) bcCML cells in wt or GPR81KO mice (GPR81 DKO). **B-D,** Leukemic burden in the bone marrow (BM) (**B**), peripheral blood (**C**), and spleen (**D**), of wt or GPR81KO bcCML initiated in wt mice, by the timepoint of wt late-stage disease (n = 5). **E-G,** Leukemic burden in the BM (**E**), peripheral blood (**F**), and spleen (**G**) at the time of wt bcCML early-stage disease, initiated using wt or GPR81KO bcCML cells in wt or GPR81KO mice (n = 4). **H,** Leukemic burden in the BM over time of wt or GPR81KO bcCML (n = 5-7). **I,** Time to progression to late-stage disease in wt or GPR81 DKO bcCML (n = 5). **J-K,** LSC repopulation assays of wt vs. *Gpr81*$^{-/-}$ bcCML cells: number of colonies at each passage (**J**), and probability of survival by passage (**K**) (n = 3, in duplicates). Significance levels determined by one-way ANOVA for **B-G,** unpaired t tests for **H**, and log-rank (Mantel-Cox) test for **I** and **K**, are indicated as: ns, not significant; *, $P < 0.05$; **, $P < 0.01$; ***, $P < 0.001$; ****, $P < 0.0001$. Error bar indicates mean ± SD.

time point of late-stage disease in wt bcCML controls (**Fig. 6B-D**). This may be attributed to the delayed rapid expansion of engrafted cells when GPR81KO bcCML cells were used; leukemic burden was near zero at the time-point of early-stage disease using wt bcCML cells (**Fig. 6E-H**). This led to an increased time to progression to >50% leukemic cells in the BM in GPR81 DKO bcCML compared to wt (**Fig. 6I**). This data suggests that leukemia cell GPR81 signaling impacts the rate of leukemia progression.

To verify the relevance of GPR81 signaling on human AML cells, analyses of publically available databases were performed. First, 163 AML patient BM samples, from The Cancer Genome Atlas (TCGA) Pan-Cancer Atlas database, were analyzed through cBioPortal for Cancer Genomics (accessed at cbioportal.org). This dataset shows a rare subset of AML patient samples with “altered”/high GPR81 (HCAR1) mRNA expression, and these patients had a median survival time of 11 months less than those with “unaltered” HCAR1 (5.03 vs 16.08 months) (**Supplementary Fig. 6A**). No gene mutations or structural variants of HCAR1 were detected in AML subjects from TCGA datasets. This suggests that mutant HCAR1 is not a contributor to AML transformation, but that dysregulation of HCAR1 expression may impact prognosis. Analysis of another dataset of BM from 707 AML patients, BeatAML 2.0 (accessed at vizome.org) (90), revealed that HCAR1 has a wider range of expression in tumor samples than in healthy BM (**Supplementary Fig. 6B**), and correlates with disease state (**Supplementary Fig. 6C**), where it is more dysregulated during initial diagnosis and relapse than during remission. There are also trends towards higher HCAR1 expression when patients had a lower survival time (**Supplementary Fig. 6D**). Together this expression data suggests that GPR81/HCAR1 expression is more dysregulated in the BMME during AML, however, it is not highly upregulated, and so suggests that the activity level of the receptor on the AML cells may be more impactful than the change in expression level.

Finally, as residual leukemic stem cells (LSCs) after chemotherapy are the primary reason for relapse in patients (34, 35), we determined the importance of GPR81 signaling to LSC potential through serial passaging in methylcellulose-containing media. The *Gpr81*$^{-/-}$ bcCML cells produced fewer colonies on average at P0 and P1 and lost repopulating capacity by P2-P3, while wt bcCML cells continue to repopulate colonies to at least P7, suggesting that GPR81 is critical to LSC capacity (**Fig. 6J** and **6K**, and **Supplementary Fig 6E**). Together,

these data display the importance of GPR81 signaling to the rapid growth and repopulation of leukemia cells.

DISCUSSION

In this research, we observe elevated levels of metabolites in the BMME during AML, defining excess lactate as a critical driver of AML-induced BMME dysfunction and leukemia progression. We identified lactate-GPR81 signaling as contributing to disease phenotypes of leukemia-associated macrophages (LAMs) and AML cells. Therefore, our results highlight the potential of GPR81 as a novel therapeutic target for both the leukemic suppression of the immune system and AML self-repopulation.

We report a global elevation of extracellular metabolites in the BMME during AML (**Fig. 1**). An amino acid-rich leukemic microenvironment was observed, in contrast to a nutrient and amino-acid-starved tumor microenvironment reported in most solid cancers (37). This distinguishes the leukemic BMME as a unique cancer microenvironment in need of further investigation. It will be useful to study how leukemia cells and BM cells utilize these metabolites, as they may act as signaling molecules or metabolic fuels. Notably, as lactate production is a hallmark of cancer, findings on the mechanisms of lactate signaling to the immune system and hematopoietic cells within the BMME are potentially applicable to multiple malignancies with BM involvement, including additional types of leukemia as well as bone metastases of solid tumors.

We demonstrate that GPR81 signaling promotes the alternative $CD206^{hi}$ phenotype observed in LAMs (**Fig. 2** and **Fig. 4**), which has been previously reported as a marker of suppressive TAMs (91). Additionally, this research identifies CD206 as a novel marker of LAMs that is unique to non-leukemia-derived macrophages. AML cells display many myeloid and macrophage markers, making them previously difficult to isolate from macrophages in the human setting; therefore, CD206 may be useful to distinguish LAMs from myeloid leukemia cells in patients. Furthermore, CD206 has been recently suggested as a prognostic factor for AML (92), and is induced on monocytes cocultured with AML blasts (69); these findings alongside our research suggest that polarization of LAMs is due to AML cell secretion of lactate, and may explain why this marker correlates with prognosis. It will be important to determine how GPR81 signaling interplays with additional signaling pathways to induce macrophage

activation, such as low pH, which has been indicated in the cooperation of lactic acid signaling with GM-CSF in the polarization of breast cancer tumor-associated macrophages (93).

LAMs have an altered transcriptome; the upregulated transcripts, as well as the cytokine release profile, suggest that they are functionally interacting with immune populations such as T cells, and secreting cytokines that have been attributed to immunosuppression, HSC development/mobilization, and tumor growth/metastasis (73, 74) (**Fig. 2** and **Supplementary Fig. 2**). This suggests a role of LAMs in the immune-privileged BMME known to occur in AML (69), which gives benefit to leukemia progression and is partially responsible for the difficulties in applying immunotherapies. More research is needed to determine if these cytokines influence the BMME through similar mechanisms and cell types as has been found in solid tumors. Furthermore, alternatively activated macrophages have been reported to induce chemotaxis/differentiation of regulatory T cells (Tregs) which further the pro-tumor microenvironment (76, 94, 95), and are inhibitory to T cells that would recognize tumor antigens (96). For example, in a breast cancer model, GPR81 signaling in the microenvironment suppressed $MHCII^{hi}$ immune cells and tumor-infiltrating T-cells, and GPR81 on tumor cells induced their expression of PD-L1 inhibitory to antigen presentation (56). Further research is needed to determine if upregulated GPR81 signaling, directly and/or through altered antigen presentation by macrophages, leads to such anti-lytic interactions between T cell populations and AML cells. The repolarization of macrophages away from a suppressive phenotype by inhibition of GPR81 may have potential in combination with current chemotherapies, or to increase the efficacy of immunotherapies, such as CAR-T cell therapy.

As AML progresses, cytopenia occurs as normal hematopoiesis is lost, secondary to alterations to the BMME, thereby leading to fatal complications of the disease. This lactate-high environment contributes to the loss of hematopoietic potential due to direct action on HSPCs, as well as through alternative polarization of macrophages (**Fig. 3**). Lactate also reduces hematopoietic support by critical HSC niche populations; stromal cells are impeded by higher levels of lactate, leading to loss of growth and differentiation to osteoblasts (**Fig. 3**). Others have found that lactate impedes osteogenic but not adipogenic differentiation of MSCs (97), suggesting a possible role of lactate in the increased adipocytic BM that contributes to a pro-tumoral BMME in AML (98).

Targeting lactate export through MCT inhibitors, and intracellular acidification, show promising results as a target for the therapeutic inhibition of AML cells (99, 100); however, the implications for hematopoietic support populations within the BMME are unknown. The lethal sensitivity that MSCs displayed experimentally to MCT inhibitors in this research raises concern for targeting this pathway therapeutically. Furthermore, prior research in the field has attempted to target various components of metabolic processes, such as lactate dehydrogenase (LDH), for the treatment of AML cells but found that it also impaired normal hematopoiesis under stress (42). This highlights the need for a therapeutic option that can selectively diminish the function of AML cells while having modest, or indeed, positive effects on the non-malignant hematopoietic and BM support populations. The experimental removal of GPR81 described herein does not negatively affect non-malignant populations, while partially rescuing the BMME (**Fig. 5**).

Relapse following chemotherapy is one of the greatest hurdles in treating AML. Our results suggest that inhibition of GPR81 may be a viable strategy to prevent the repopulation of AML cells following treatment; autocrine lactate signaling through GPR81 has been described in solid tumors, and we find it as a critical receptor to bcCML cells for disease kinetics and repopulating ability (**Fig. 6**). The signaling pathways downstream of GPR81 are numerous, and multiple pathways have been investigated in cancer cell metabolism, DNA repair, and chemoresistance (52-54). Defining the signaling pathways downstream of GPR81 in AML and other hematopoietic malignancies is promising for the identification of additional mechanisms to target LSCs in the BM. Lastly, the development of a selective molecule to this receptor is strongly supported by our findings, as there is currently no selective GPR81 antagonist available. In conclusion, this research suggests that targeting GPR81 signaling in the BMME during AML may be a selective and well-tolerated therapeutic option to prevent LSC repopulation and rescue microenvironmental dysfunction.

METHODS

Human Bone Marrow Extracellular Fluid Collection

Deidentified bone marrow aspirates were collected from patients, and immediately centrifuged to pellet cells. Following separation, the supernatant was stored at -80C until use.

Metabolomics

Bone marrow extracellular fluid samples were thawed at room temp and briefly mixed, then immediately kept on ice. Sample dilutions were prepared by mixing 20 µl sample and 280 µl cold 80:20 HPLC-grade MeOH:water (Omnisolv MeOH MX0488-1; Omnisolv water WX0004-1) and briefly vortexed. Diluted samples were centrifuged at 4°C, at 16000 x g for 10 min to pellet precipitate, and the resulting supernatants were transferred to new tubes. For all amino acids, samples underwent carbobenzyloxy (CBZ) derivatization by mixing 90 µl of diluted sample, 5 µl trimethylamine (Sigma #471283), and 1 µl benzyl chloroformate (Acros 152940050). Tubes were incubated at room temp for 5 min then centrifuged at 16000 xg for 10 min, and supernatants were transferred to HPLC vials. LC-MS/MS was performed using an LC-20AD HPLC system (Shimadzu). For amino acids, a Synergi 4 µm Hydro-RP 80A 50x2mm column (Phenomenex 00B-4375-B0) was utilized with the following LC parameters: autosampler temperature, 4 °C; injection volume, 10 µL; column temperature, 40 °C; and flow rate, 0.5 mL/min. The LC solvents used were: solvent A, 100% methanol; and solvent B, 10 mM tributylamine and 15 mM acetic acid in 97:3 (vol:vol) water:methanol. The gradient conditions used were (vol/vol): negative mode-t = 0, 85% B; t = 4, 3%B; t = 5, 3% B; t = 5.1, 85% B. For all non-amino acid metabolites, 100 µl of methanol extracts were cleared by centrifugation as above, transferred to HPLC vials, and 10 µL injected. These extracts were run over a Synergi 4 µm hydro-RP 80A 150x2mm HPLC column (Phenomenex 00F-4375-B0). The total run time was 20 min, with solvent A being 97:3 water/methanol with 10 mM tributylamine and 15 mM acetic acid; and solvent B being methanol. The gradient was 0 min, 0% B, flow rate 200 µL/min; 2.5 min, 0% B, flow rate 200 µL/min; 5 min, 20% B, flow rate 250 µL/min; 12 min, 95% B, flow rate 250 µL/min; 14.5 min, 95% B, flow rate 250 µL/min; 15 min, 0% B, flow rate 250 µL/min; 19 min, 0% B, flow rate 200 µL/min; 20 min, 0% B, flow rate 200 µL/min. Mass-spectrometric analyses were performed on a TSQ Quantum Ultra triple-quadrupole mass spectrometer running in multiple reaction monitoring mode (Thermo Fisher Scientific). Peak heights for metabolite chromatograms were analyzed by using the Xcalibur software.

Data Processing and Analyses: Raw Xcalibur data was transformed to peak intensity (relative abundance) of known compounds using mzRock analysis software

(https://code.google.com/archive/p/mzrock/). Compound prediction reports were used to manually filter any trace detection (use only those with aligned retention time, intensity >10000). MetaboAnalyst 5.0 software was used to process the peak intensity data, perform the statistical analysis, and generate heatmaps, as described in **Supplementary Methods**.

Murine Strains and Disease Models

All murine experiments were performed using male and female wild type C57BL/6J mice obtained from the Jackson Laboratory. Previous studies from our lab and others have shown no sex-dependent differences in the BMME in the number of HSCs, mesenchymal stem cells (MSCs), macrophages, endothelial cells, osteoblastic cells (OBs), or the immunohistochemistry involved. The male and female data were plotted together unless a sex-specific difference was noted. All mice were maintained by monogamous breeding and housed pathogen-free at the Vivarium at the University of Rochester School of Medicine and Dentistry. All facilities and animal care comply with federal and NIH policies, accredited by the Association for Assessment and Accreditation of Laboratory Animal Care International (AAALAC).

Gpr81$^{-/-}$ mice, genetically modified to lack a functional gene for the receptor GPR81/HCAR1, previously characterized and used for published studies: They were kindly acquired via material transfer agreement from Dr. Vadivel Ganapathy, Ph.D. (professor and department chair of cell biology and biochemistry at Texas Tech University Health Sciences Center, U.S.), who obtained the mice from Dr. Stefan Offermanns (professor and director of the department of pharmacology at Max-Planck-Institute for Heart and Lung Research, Germany). Mice were on a B6 (>10 generation) background (101). Dr. Offermanns originally procured the mice from the Texas Institute of Genomic Medicine (Houston, TX, U.S.) (102).

Experiments were performed using the following murine model of AML:
A previously established model of blast crisis chronic myelogenous leukemia (bcCML) (29, 66, 82), an acutely progressing malignancy resulting in the accumulation of myeloid blasts in the BM. Primary bcCML was initiated via tail vein injection of bcCML cells into 8–12-week-old mice sublethally irradiated with 6.5 gray (Gy). Leukemic cells were generated by retroviral

transduction of hematopoietic stem and progenitor cells (HSPCs) with MSCV vectors containing the following gene translocation fusion-products common to myeloid leukemia: the constitutively active mitogenic kinase BCR-ABL (BA) conjugated to green fluorescent protein (GFP) via IRES for experimental detection, and the HSC-related transcription factor fused to a nuclear translocation protein Nup98-HoxA9 (NH) conjugated to yellow fluorescent protein (YFP). The BA-NH leukemic cells engraft in the BM and then expand. Spleen cells were harvested from these primary leukemic mice and stored in liquid nitrogen until use for secondary initiation of bcCML used for experiments. Myeloablative radiation is not necessary before secondary injection. This AML model progresses to end-stage leukemia within 12-18 days in wt mice. For comparative bcCML *in vivo* experiments, 10,000 wt or *Gpr81*$^{-/-}$ bcCML cells per 100 µL dose were injected into age- and sex-matched wt or *Gpr81*$^{-/-}$ mice.

Leukemic Plasmid Production and Purification

Bacterial stocks containing the BA or NH gene in an ampicillin-resistance plasmid were created from bacteria transfected for previous publications. Bacteria were streaked on LB-agar plates with ampicillin and single colonies were picked to grow in LB-broth with ampicillin overnight. Bacteria were pelleted and plasmids were extracted using a NucleoBond Xtra Maxi kit (Macherey-Nagel).

Transfection of PLAT-E Cells for Retrovirus Production

Cells from the Platinum-E (PLAT-E) retroviral packaging cell line (ATCC) were grown in complete DMEM in culture-treated T-75 flasks, then lifted using 0.25% trypsin, and replated on fibronectin-coated six-well culture dishes, then grown overnight without antibiotics. Media was changed and a calcium phosphate transfection was performed using 10 µg of plasmid per well. Media was changed after 24 hours, then cells were incubated for an additional 24 hours. Viral supernatant was then collected and snap-frozen in liquid nitrogen, then stored at -80°C until use.

Flow Cytometry and Fluorescence-Activated Cell Sorting (FACS)

All samples were resuspended in 1X phosphate-buffered saline (PBS) (Corning 21-040-CV) with added 2% heat-inactivated fetal bovine serum (htFBS) (Gibco 26140079, heat-treated at

56°C for 30 min). All antibodies for flow cytometry and cell sorting were obtained commercially. See **Supplementary Methods Table 1 (Table SM1)** for a list of flow cytometry antibodies and **Supplementary Methods Table 2 (Table SM2)** for markers and gating strategies used. Fluorescence minus one (FMO), and positive controls prepared using UltraComp eBeads compensation beads (Invitrogen 01-2222-42), were used in each experiment to ensure accurate staining and appropriate gating. Only the live, single cells were considered in analyses, where single cells were determined by side scatter and forward scatter, and live cells were detected by DAPI live/dead nuclear stain. Flow cytometric analyses were performed at the University of Rochester Wilmot Cancer Center on an LSRFortessa Cell Analyzer (BD Biosciences), and FACS was performed at the Flow Cytometry Core at the University of Rochester Medical Center on a FACSAria II system (BD Biosciences) with an 85-micron nozzle at 4°C, using FACSDiva software (BD Biosciences), and then analyzed using FlowJo v10 software (BD Biosciences).

Viral Transfection of HSPCs for bcCML Cell Production

HSPCs were sorted via FACS and cultured overnight in media with added “LSK cytokines” to promote maintenance of stemness *in vitro* (LSK media = complete MEM α with recombinant murine cytokines: 50 ng/mL of SCF (PeproTech 250-03) and Flt3-Ligand (PeproTech 250-31L), and 10 ng/mL of IL-3 (PeproTech 213-13) and IL-6 (PeproTech 216-16) in a 24-well suspension plate. The entire well was collected and centrifuged, the supernatant was removed, and then cells HSPCs were resuspended in LSK media containing double the concentration of LSK cytokines, diluted with an equal volume of viral supernatant on retronectin-coated dishes (Takara). Media and viral supernatant were replaced 2x per day for two additional days, and 1x on the third morning. Six hours later, the cells were collected and resuspended in 1X PBS with 2% htFBS for injection.

Murine Bone Marrow Extracellular Fluid Collection

Tibias and femurs were dissected and crushed in 1 mL of 1X PBS. This cellular suspension was then filtered through a 40 µm cell strainer into a 50 mL conical tube to remove bone fragments. The cells were pelleted by centrifugation at 900 x g for five minutes and the supernatant was removed into an Eppendorf tube, then immediately stored at -80C until use.

Lactate Measurements

Lactate concentrations were measured from BM extracellular fluid samples using a colorimetric lactate assay kit (Sigma MAK064) and absorbance was read on a BioTek Synergy 2 multi-mode microplate reader according to the manufacturer's instructions.

Murine Complete Blood Counts (CBCs)

Blood samples were collected from mice by submandibular bleeds into BD Microtainer tubes with K2E (K_2EDTA) (BD Biosciences #365974). CBCs were performed on 10 µl of blood using a scil Vet abc Plus hematology analyzer (Antech).

Whole Bone Marrow Isolation from Mice

6-12-week-old mice were euthanized by carbon dioxide asphyxiation followed by cervical dislocation. Mice were briefly dipped before dissection into a container of 70% ethanol (200-proof ethanol (VWR 89125-174) diluted using distilled water (dH_20). The hindlimbs (tibias and femurs) were removed by dissection, and the muscles were removed from the outside of the bone by dissection followed by rubbing with a Kimtech Kimwipe (Kimberly-Clark 34256). The bones were crushed in 1X PBS using a pestle and mortar to remove the BM, then filtered through a 40 µM cell strainer into a 50 mL conical tube to remove bone fragments. The cells were pelleted by centrifugation at 900 x g for five minutes and the supernatant was removed.

Red Blood Cell Lysis

Whole bone marrow freshly isolated from mice was resuspended in red blood cell lysis buffer (156 mM NH_4CL (Sigma 213330-25G), 127 µM EDTA (Sigma E4884-100G), and 12 mM $NaHCO_3$ (Sigma S6014-25G) in dH_20 (all dH_20 for cellular or molecular work was purified by use of a Barnstead Nanopure system (Thermo Fisher Scientific)) for five minutes to lyse the red blood cells before flow cytometry analysis. Cells are resuspended in a greater amount of 1X PBS then centrifuged to the pellet, and the lysis buffer is removed.

Simplified Presentation of Incredibly Complex Evaluations (SPICE)

The SPICE analysis was performed using SPICE 6 software publicly available through the NIH NIAID site.

Bulk RNA Sequencing (RNAseq)

RNA sequencing and analysis were performed by the University of Rochester Genomics Research Center. See **Supplementary Methods** for details.

Macrophage Cytokine ELISA

To identify differential cytokines secreted by LAMs and normal macrophages: A stromal monolayer of murine whole bone marrow was grown in complete to confluency in “complete” (with 10% htFBS and 1x antibiotic-antimycotic (anti-anti) (Gibco 15240062)) Minimum Essential Medium α (MEM α) (with nucleosides and L-glutamine, without ascorbic acid, Gibco A10490-01). Macrophages were then sorted from nonleukemic mice or LAMs were sorted from bcCML mice via FACS. The macrophages were cocultured in the stromal monolayer dish for 4 days to establish a microenvironment, then the cell culture media was collected and stored immediately at -20C until use. The Proteome Profiler Mouse XL Cytokine Array (Bio-Techne R and D systems ARY028) was used according to manufacturer protocol to perform an ELISA for a variety of cytokines. The blot was imaged using the ChemiDoc MP Imaging System (BioRad) and Image Lab software (BioRad) on the western blot high sensitivity setting for automatic exposure. Images were equally adjusted for background and the blot was qualitatively assessed for cytokine presence.

Bone Marrow-Derived Macrophages (BMDM) Production

Whole BM was plated in a vented tissue culture-treated 75cm^2 flask (NEST 708001) overnight in complete Dulbecco’s Modified Eagle Medium (DMEM) (Corning 10-013-CV). The next day, all non-adherent cells were transferred in the same culture media to be plated on 12-well cell culture dishes at 400K cells/well in 1 mL + recombinant murine macrophage colony-stimulating factor (M-CSF) (PeproTech 315-02), plus any treatment conditions. Media was changed on day 4 including stimuli/lactate, and differentiation to BMDMs was complete by day 7, where cells were either treated or grown/passaged up to P1.

Macrophage Polarization Experiments

Treatment groups were serum-starved for 6 hours before treatment (DMEM, anti-anti, and M-CSF without htFBS), and treatment conditions (100 ng/mL lipopolysaccharides (LPS) from E. coli O55:B5 (Sigma L6529), or 5 ng/mL of recombinant murine interleukin (IL) -4 and -13 (IL-4, IL-13) (ILs) (PeproTech 214-14, 210-13), were added to the serum-free media. To remove cells for flow analysis, 0.25% trypsin-EDTA (Gibco 25200056) was added for 5 min then cell scrapers were used to dislodge cells. Additional syrosingopine (Sigma SML 1908 resuspended in DMSO) treatments were done at 5 µM. To determine if this polarization is reversible, we treated BMDMs with the polarization stimuli for 24 hours, then changed to fresh media and cultured for one week. Stromal monolayer polarization was done similarly to BMDM polarization, with 5 ng/mL of ILs and 10 mmol/L of lactate.

Quantitative Real-Time Polymerase Chain Reaction (qRT-PCR)

Cells were grown to 70% confluency in corresponding media in tissue culture-treated 12-well plates. Media was changed to serum-free media for 12-24 hours before lactate treatment. Lactate was added to wells at 10 mmol/L and cells were cultured for the desired time. For BMDMs 5 ng/mL of IL4 and IL13 was also added to stimulate polarization. Wells were treated for 0, 1, 2, 4, 6, or 9 hours, and cells were then removed from the well by treatment with 0.25% trypsin-EDTA for three minutes then by the additional use of a cell-scraper for macrophage cultures. All cells were collected in an Eppendorf tube and centrifuged at 3000 x g for 3 minutes to pellet the cells. The supernatant was removed, and cells were resuspended in RLT lysis buffer (Qiagen), then stored at -20C until RNA extraction by RNeasy Plus Mini Kit (Qiagen 74134). The cDNA libraries were then prepared using the High-Capacity cDNA Reverse Transcription kit (Applied Biosystems, ThermoFisher 4368814). The TaqMan Gene Expression Master Mix (ThermoFisher 4369016) was used for qRT-PCR along with the following TaqMan Gene Expression Assays (FAM) (ThermoFisher 4331182): Gpr81/Hcar1 mouse (Mm00558586_s1), Mct1 mouse (Mm01306379_m1), Mct4 mouse (Mm01246825_m1), Arg1 mouse (Mm00475988_m1), iNOS mouse (Mm00440502_m1), and beta-actin mouse (Mm04394036_g1). The assay was run on the QuantStudio 12KFlex Real-Time PCR System at the UR Genomics Research Center. The relative quantification (RQ) of mRNA expression was calculated using the $2^{-(\Delta\Delta Ct)}$ method (Ct = cycle threshold).

Colony Forming Units (CFU-C) Assays for HSPC Potential

LSK with Stromal Monolayer: Whole BM freshly isolated from mice was plated on six-well cell culture-treated dishes at $4x10^6$ cells per well in complete MEM α without ascorbic acid. Cells were grown overnight, then non-adherent cells were removed from the dish and fresh media was added. Cells were grown to confluency, with media aspirated and fresh media added every 3 - 4 days. LSKs were sorted via FACS and added on day 14 in LSK media. The cocultures were incubated for 72 hours and then plated for colony-forming units CFU-Cs (see below).

LSK Only: These were cultured for 48-72 hours in a sterile 24-well suspension culture plate (CELLSTAR 622102, Greiner Bio-One) in LSK media with varying lactate treatments, then plated for CFU-Cs.

With Added LAMs: macrophages were obtained by FACS from the BM of either leukemic mice or non-leukemic control mice and plated into the wells to grow for 4 days. Then, LSKs were sorted from freshly isolated mouse BM, and 500 cells per well were added to the stromal coculture support layer. These were cultured for four days in LSK media with or without lactate added, then plated for (CFU-C).

To plate cells for CFU-Cs, all cells were collected from the wells by collecting the media with non-adherent cells in a 15 mL conical tube, and then using 0.25% trypsin-EDTA on the adherent cells for five minutes then flushing the wells with fresh MEM α and adding it to the tube. Cells were pelleted by centrifugation for five minutes at 900 x g. Then, cells were resuspended in 0.5 mL of MEM α. From here, both 1:20 and 1:100 dilutions were made in 2.5 mL of media in separate Eppendorf tubes. Then, 0.2 mL of these dilutions were resuspended each in 2.5 mL aliquots of MethoCult (StemCell Technologies M3434) methylcellulose-containing media and immediately plated in duplicates of 1.2 mL into 35mm x 10mm sterile suspension culture dishes (Corning 430588). These were placed inside a sterile 150 mm x 25 mm dish (NEST 715001), with one open dish of sterile dH_20 in the center to retain humidity

and prevent drying of the cultures. These were incubated for 10-14 days (5% CO_2; 37C), then colonies were counted using a microscope.

Colony Forming Unit-Osteoblast (CFU-OB) Assay

Whole BM from mice were plated at 4 x 10^6 cells per well in tissue culture-treated 6-well plates, or at 2 x 10^6 cells per well in 12-well plates, in ascorbic acid-free MEM α at 37°C, 5%CO2. After attachment overnight, media with nonadherent cells was removed, and fresh media was added. On day four, the media was changed to mineralizing media (complete MEM α without ascorbic acid was used as a media base, with added 0.05 mg/mL L-ascorbic acid (Krackeler 45-A4544) and 10mM glycerol 2-phosphate disodium salt hydrate (Krackeler G9422) then sterile-filtered (NEST 343011). Cells were treated with 0, 5, 10, or 15 mmol/L of excess lactate starting on day 4, and incubated for 14 days, with media changed every three days. The attached cells were fixed with 10% neutral buffered formalin for 20 minutes and then rinsed with dH_20. Triplicate wells were assayed for alkaline phosphatase activity, indicating pre-osteoblasts (Pre-OB), by staining for 45 minutes with a solution of 100 mM Tris-HCl, 0.005% weight/volume naphthol AS MX-PO4, and 0.03% weight/volume red violet LB salt. To assay for silver nitrate-positive colonies, cultures were grown until day 28, and then Von Kossa staining was done by staining for alkaline phosphatase followed by three rinses with dH_20 and then 2.5% silver nitrate solution for 30 minutes. After staining, wells were then rinsed with dH_20 and allowed to dry. Plates were imaged using a high-definition scanner (Canon), and then images were analyzed for area by color thresholding using ImageJ image analysis software (NIH).

Colony Forming Unit-Fibroblast (CFU-F) and MSC Proliferation Assays

Whole BM from mice were plated at P0 at 2 x 10^6 cells per well in tissue culture-treated 12-well plates in ascorbic acid-free MEM α at 37°C, 5% CO2. Cells were treated with 0, 5, 10, or 15 mmol/L of excess lactate starting on day 4, and incubated for 10-14 days, with media changed every three days. Any syrosingopine treatments were done at 1 µM. The attached cells were fixed with 10% neutral buffered formalin for 20 minutes, then rinsed with dH_20. Wells were stained with a 50/50 mix of 1% crystal violet dissolved in 100% methanol for 30 minutes, rinsed with dH_20 three times, and left in water overnight. To quantify crystal violet

staining, the water was removed and rinsed, then the crystal violet stain was solubilized in 300 µl of 10% acetic acid in dH20 for 15 minutes, then diluted 1:2 in dH_20, and the absorbance was read at A = 590 nm on the microplate reader.

Analysis of RNA and Protein Expression from Publicly Available Databases

Accessed via cbioportal.org and queried for HCAR1 in AML from the TCGA PanCancer Atlas and Firehose Legacy databases. The mRNA expression alternate group was set for RNA Seq V2 RSEM z score $\pm$ 2, where z-scores were compared to the expression distribution of each gene tumors that are diploid for this gene.

Leukemia Stem Cell (LSC) Assay

Doubly-transfected (GFP^+, YFP^+) bcCML cells were sorted by FACS from the wt or *Gpr81*$^{-/-}$ bcCML primary spleen cell frozen stocks. Cells were plated at passage 0 (P0) in MethoCult as described in CFU-C assays. After 10-14 days, four well-established colonies were picked, resuspended in 200 µl of media, and replated at two dilutions. This continued until colonies did not appear, or the seventh passage (P7) was reached.

Rigor and Statistical Analysis

All human and mouse samples were age- and sex-matched to control samples. Experiments were replicated at least three times. Sample size analyses have been performed on all preliminary data to ensure that subsequent repetitions were appropriately powered. All metabolomics analysis was computed using MetaboAnalyst 5.0 software, as indicated in **Supplementary Methods**. Other statistical analyses were performed using GraphPad Prism 10 software.

Human Specimens

All human specimens have been previously obtained on IRB-approved protocols and were de-identified.

Data Availability Statement

The metabolomics and RNAseq datasets generated and analyzed during the study, and any other raw data, were made available from the corresponding author upon request.

Authors' Contributions

C. A. Soto: Conceptualization, experiments, data analysis, methodology, writing, and editing. **M. L. Lesch, A. Sharipol, and A. Khan:** assisted in experiments. **X. L. Schafer:** assisted with LC/MS-MS training and analysis. **M. W. Becker:** human samples and conceptualization. **J. C. Munger:** Conceptualization, methodology, and data analysis. **B. J. Frisch:** Conceptualization, data analysis, methodology, reviewing/editing, and oversight of the project.

Acknowledgments

The human BM aspirate samples were obtained by Dr. Michael Becker, MD, and the bcCML model bacterial plasmids come from the lab of Dr. Laura Calvi, MD, of the Wilmot Cancer Institute. We thank Dr. Vadivel Ganapathy, Ph.D. at Texas Tech University for sending the *Gpr81*$^{-/-}$ mice. The RNA sequencing and analysis were performed by the Genomics Research Center at the University of Rochester Medical Center. We thank Dr. Helene McMurray, Ph.D., of the Cell Biology of Disease Program at the University of Rochester School of Medicine and Dentistry for insight on accessing and analyzing publicly available data from cancer patient databases. We thank Dr. Danielle Benoit, Ph.D., Dr. Roman Eliseev, MD, Ph.D., and Dr. Omar Ajiltawi, MD, as well as lab members from the labs of Dr. Laura Calvi, MD and Dr. Jane Liesveld, MD, Yuko Kawano, MD, PhD, Mark LaMere, and Mitra Azadniv, PhD, of the University of Rochester Medical Center for their feedback and assistance during the development of the project. This work was supported in part by the Wilmot Cancer Institute Research Development Funding Program Award to Dr. Frisch and Dr. Munger, Dr. Frisch's institutional start-up funding, and by a National Research Service Award (NRSA) Institutional Research Training Grant (T32) from the NIH to Celia Soto through the Rochester Musculoskeletal (ROCMSK) Training Program at the University of Rochester Center for Musculoskeletal Research (CMSR).

References

1. Ferrara F, Schiffer CA. Acute myeloid leukaemia in adults. The Lancet. 2013;381(9865):484-95.
2. Crossnohere NL, Richardson DR, Reinhart C, O'Donoghue B, Love SM, Smith BD, et al. Side effects from acute myeloid leukemia treatment: results from a national survey. Current Medical Research and Opinion. 2019;35(11):1965-70.
3. Thol F, Ganser A. Treatment of Relapsed Acute Myeloid Leukemia. Current Treatment Options in Oncology. 2020;21(8):66.
4. Gupta V, Tallman MS, Weisdorf DJ. Allogeneic hematopoietic cell transplantation for adults with acute myeloid leukemia: myths, controversies, and unknowns. Blood. 2011;117(8):2307-18.
5. Yi M, Li A, Zhou L, Chu Q, Song Y, Wu K. The global burden and attributable risk factor analysis of acute myeloid leukemia in 195 countries and territories from 1990 to 2017: estimates based on the global burden of disease study 2017. Journal of Hematology & Oncology. 2020;13(1):72.
6. Döhner H, Weisdorf DJ, Bloomfield CD. Acute Myeloid Leukemia. New England Journal of Medicine. 2015;373(12):1136-52.
7. Chang H-Y, Rodriguez V, Narboni G, Bodey GP, Luna MA, Freireich EJ. CAUSES OF DEATH IN ADULTS WITH ACUTE LEUKEMIA. Medicine. 1976;55(3).
8. Miraki-Moud F, Anjos-Afonso F, Hodby KA, Griessinger E, Rosignoli G, Lillington D, et al. Acute myeloid leukemia does not deplete normal hematopoietic stem cells but induces cytopenias by impeding their differentiation. Proceedings of the National Academy of Sciences of the United States of America. 2013;110(33):13576-81.
9. Till JE, McCulloch EA. A Direct Measurement of the Radiation Sensitivity of Normal Mouse Bone Marrow Cells. Radiation Research. 1961;14(2):213-22.
10. Schofield R. The relationship between the spleen colony-forming cell and the haemopoietic stem cell. Blood Cells. 1978;4(1-2):7-25.
11. Frisch BJ. The hematopoietic stem cell niche: What's so special about bone? Bone. 2019;119:8-12.
12. Asada N, Kunisaki Y, Pierce H, Wang Z, Fernandez Nicolas F, Birbrair A, et al. Differential cytokine contributions of perivascular haematopoietic stem cell niches. Nature Cell Biology. 2017;19(3):214-23.
13. Greenbaum A, Hsu Y-MS, Day RB, Schuettpelz LG, Christopher MJ, Borgerding JN, et al. CXCL12 in early mesenchymal progenitors is required for haematopoietic stem-cell maintenance. Nature. 2013;495(7440):227-30.
14. Méndez-Ferrer S, Michurina TV, Ferraro F, Mazloom AR, MacArthur BD, Lira SA, et al. Mesenchymal and haematopoietic stem cells form a unique bone marrow niche. Nature. 2010;466(7308):829-34.
15. Calvi LM, Adams GB, Weibrecht KW, Weber JM, Olson DP, Knight MC, et al. Osteoblastic cells regulate the haematopoietic stem cell niche. Nature. 2003;425(6960):841-6.
16. Zhang J, Niu C, Ye L, Huang H, He X, Tong W-G, et al. Identification of the haematopoietic stem cell niche and control of the niche size. Nature. 2003;425(6960):836-41.
17. Zhu J, Garrett R, Jung Y, Zhang Y, Kim N, Wang J, et al. Osteoblasts support B-lymphocyte commitment and differentiation from hematopoietic stem cells. Blood. 2007;109(9):3706-12.

18. Bowers M, Zhang B, Ho Y, Agarwal P, Chen C-C, Bhatia R. Osteoblast ablation reduces normal long-term hematopoietic stem cell self-renewal but accelerates leukemia development. Blood. 2015;125(17):2678-88.
19. Green AC, Tjin G, Lee SC, Chalk AM, Straszkowski L, Kwang D, et al. The characterization of distinct populations of murine skeletal cells that have different roles in B lymphopoiesis. Blood. 2021.
20. Kunisaki Y, Bruns I, Scheiermann C, Ahmed J, Pinho S, Zhang D, et al. Arteriolar niches maintain haematopoietic stem cell quiescence. Nature. 2013;502(7473):637-43.
21. Acar M, Kocherlakota KS, Murphy MM, Peyer JG, Oguro H, Inra CN, et al. Deep imaging of bone marrow shows non-dividing stem cells are mainly perisinusoidal. Nature. 2015;526(7571):126-30.
22. Fang S, Chen S, Nurmi H, Leppänen V-M, Jeltsch M, Scadden D, et al. VEGF-C protects the integrity of the bone marrow perivascular niche in mice. Blood. 2020;136(16):1871-83.
23. Chow A, Lucas D, Hidalgo A, Méndez-Ferrer S, Hashimoto D, Scheiermann C, et al. Bone marrow CD169+ macrophages promote the retention of hematopoietic stem and progenitor cells in the mesenchymal stem cell niche. Journal of Experimental Medicine. 2011;208(2):261-71.
24. Fujisaki J, Wu J, Carlson AL, Silberstein L, Putheti P, Larocca R, et al. In vivo imaging of Treg cells providing immune privilege to the haematopoietic stem-cell niche. Nature. 2011;474(7350):216-9.
25. Sugiyama T, Kohara H, Noda M, Nagasawa T. Maintenance of the Hematopoietic Stem Cell Pool by CXCL12-CXCR4 Chemokine Signaling in Bone Marrow Stromal Cell Niches. Immunity. 2006;25(6):977-88.
26. Staversky RJ, Byun DK, Georger MA, Zaffuto BJ, Goodman A, Becker MW, et al. The Chemokine CCL3 Regulates Myeloid Differentiation and Hematopoietic Stem Cell Numbers. Sci Rep. 2018;8(1):14691.
27. Sitnicka E, Lin N, Priestley G, Fox N, Broudy V, Wolf N, et al. The effect of thrombopoietin on the proliferation and differentiation of murine hematopoietic stem cells. Blood. 1996;87(12):4998-5005.
28. Arai F, Hirao A, Ohmura M, Sato H, Matsuoka S, Takubo K, et al. Tie2/angiopoietin-1 signaling regulates hematopoietic stem cell quiescence in the bone marrow niche. Cell. 2004;118(2):149-61.
29. Frisch BJ, Ashton JM, Xing L, Becker MW, Jordan CT, Calvi LM. Functional inhibition of osteoblastic cells in an in vivo mouse model of myeloid leukemia. Blood. 2012;119(2):540-50.
30. Goncalves KA, Silberstein L, Li S, Severe N, Hu MG, Yang H, et al. Angiogenin Promotes Hematopoietic Regeneration by Dichotomously Regulating Quiescence of Stem and Progenitor Cells. Cell. 2016;166(4):894-906.
31. Winkler IG, Barbier V, Nowlan B, Jacobsen RN, Forristal CE, Patton JT, et al. Vascular niche E-selectin regulates hematopoietic stem cell dormancy, self renewal and chemoresistance. Nat Med. 2012;18(11):1651-7.
32. Kode A, Manavalan JS, Mosialou I, Bhagat G, Rathinam CV, Luo N, et al. Leukaemogenesis induced by an activating β-catenin mutation in osteoblasts. Nature. 2014;506(7487):240-4.
33. Soto CA, Lo Celso C, Purton LE, Frisch BJ. From the niche to malignant hematopoiesis and back: reciprocal interactions between leukemia and the bone marrow microenvironment. JBMR Plus. 2021;5(10):e10516.
34. Ishikawa F, Yoshida S, Saito Y, Hijikata A, Kitamura H, Tanaka S, et al. Chemotherapy-resistant human AML stem cells home to and engraft within the bone-marrow endosteal region. Nature Biotechnology. 2007;25(11):1315-21.
35. Lapidot T, Sirard C, Vormoor J, Murdoch B, Hoang T, Caceres-Cortes J, et al. A cell initiating human acute myeloid leukaemia after transplantation into SCID mice. Nature. 1994;367(6464):645-8.

36. Isidori A, Cerchione C, Daver N, DiNardo C, Garcia-Manero G, Konopleva M, et al. Immunotherapy in Acute Myeloid Leukemia: Where We Stand. Frontiers in Oncology. 2021;11.
37. Bader JE, Voss K, Rathmell JC. Targeting Metabolism to Improve the Tumor Microenvironment for Cancer Immunotherapy. Molecular Cell. 2020;78(6):1019-33.
38. Baltazar F, Afonso J, Costa M, Granja S. Lactate Beyond a Waste Metabolite: Metabolic Affairs and Signaling in Malignancy. Frontiers in Oncology. 2020;10.
39. Bejarano L, Jordão MJC, Joyce JA. Therapeutic Targeting of the Tumor Microenvironment. Cancer Discov. 2021;11(4):933-59.
40. Elia I, Haigis MC. Metabolites and the tumour microenvironment: from cellular mechanisms to systemic metabolism. Nature Metabolism. 2021;3(1):21-32.
41. Warburg O. On the origin of cancer cells. Science. 1956;123(3191):309-14.
42. Wang Y-H, Israelsen William J, Lee D, Yu Vionnie WC, Jeanson Nathaniel T, Clish Clary B, et al. Cell-State-Specific Metabolic Dependency in Hematopoiesis and Leukemogenesis. Cell. 2014;158(6):1309-23.
43. Rogatzki MJ, Ferguson BS, Goodwin ML, Gladden LB. Lactate is always the end product of glycolysis. Frontiers in Neuroscience. 2015;9.
44. Brooks GA, Dubouchaud H, Brown M, Sicurello JP, Butz CE. Role of mitochondrial lactate dehydrogenase and lactate oxidation in the intracellular lactate shuttle. Proceedings of the National Academy of Sciences. 1999;96(3):1129-34.
45. de la Cruz-López KG, Castro-Muñoz LJ, Reyes-Hernández DO, García-Carrancá A, Manzo-Merino J. Lactate in the Regulation of Tumor Microenvironment and Therapeutic Approaches. Frontiers in oncology. 2019;9:1143-.
46. Walenta S, Wetterling M, Lehrke M, Schwickert G, Sundfør K, Rofstad EK, et al. High lactate levels predict likelihood of metastases, tumor recurrence, and restricted patient survival in human cervical cancers. Cancer Res. 2000;60(4):916-21.
47. Ritzhaupt A, Wood IS, Ellis A, Hosie KB, Shirazi-Beechey SP. Identification and characterization of a monocarboxylate transporter (MCT1) in pig and human colon: its potential to transport l-lactate as well as butyrate. The Journal of Physiology. 1998;513(3):719-32.
48. DIMMER K-S, FRIEDRICH B, LANG F, DEITMER JW, BRÖER S. The low-affinity monocarboxylate transporter MCT4 is adapted to the export of lactate in highly glycolytic cells. Biochemical Journal. 2000;350(1):219-27.
49. De Saedeleer CJ, Copetti T, Porporato PE, Verrax J, Feron O, Sonveaux P. Lactate Activates HIF-1 in Oxidative but Not in Warburg-Phenotype Human Tumor Cells. PLOS ONE. 2012;7(10):e46571.
50. Viola A, Munari F, Sánchez-Rodríguez R, Scolaro T, Castegna A. The Metabolic Signature of Macrophage Responses. Frontiers in Immunology. 2019;10.
51. li X, Chen Y, Wang T, Liu Z, Yin G, Wang Z, et al. GPR81-mediated reprogramming of glucose metabolism contributes to the immune landscape in breast cancer. Discover Oncology. 2023;14(1):140.
52. Ishihara S, Hata K, Hirose K, Okui T, Toyosawa S, Uzawa N, et al. The lactate sensor GPR81 regulates glycolysis and tumor growth of breast cancer. Scientific Reports. 2022;12(1):6261.
53. Roland CL, Arumugam T, Deng D, Liu SH, Philip B, Gomez S, et al. Cell surface lactate receptor GPR81 is crucial for cancer cell survival. Cancer Res. 2014;74(18):5301-10.
54. Wagner W, Kania KD, Blauz A, Ciszewski WM. The lactate receptor (HCAR1/GPR81) contributes to doxorubicin chemoresistance via abcb1 transporter up-regulation in human cervical cancer hela cells. Journal of Physiology and Pharmacology. 2017;68(4):555-64.

55. Feng J, Yang H, Zhang Y, Wei H, Zhu Z, Zhu B, et al. Tumor cell-derived lactate induces TAZ-dependent upregulation of PD-L1 through GPR81 in human lung cancer cells. Oncogene. 2017;36(42):5829-39.
56. Brown TP, Bhattacharjee P, Ramachandran S, Sivaprakasam S, Ristic B, Sikder MOF, et al. The lactate receptor GPR81 promotes breast cancer growth via a paracrine mechanism involving antigen-presenting cells in the tumor microenvironment. Oncogene. 2020;39(16):3292-304.
57. Gordon S, Martinez FO. Alternative Activation of Macrophages: Mechanism and Functions. Immunity. 2010;32(5):593-604.
58. Zhang QW, Liu L, Gong CY, Shi HS, Zeng YH, Wang XZ, et al. Prognostic significance of tumor-associated macrophages in solid tumor: a meta-analysis of the literature. PLoS One. 2012;7(12):e50946.
59. Zhang Q, He Y, Luo N, Patel SJ, Han Y, Gao R, et al. Landscape and Dynamics of Single Immune Cells in Hepatocellular Carcinoma. Cell. 2019;179(4):829-45.e20.
60. Colegio OR, Chu N-Q, Szabo AL, Chu T, Rhebergen AM, Jairam V, et al. Functional polarization of tumour-associated macrophages by tumour-derived lactic acid. Nature. 2014;513(7519):559-63.
61. Mu X, Shi W, Xu Y, Xu C, Zhao T, Geng B, et al. Tumor-derived lactate induces M2 macrophage polarization via the activation of the ERK/STAT3 signaling pathway in breast cancer. Cell Cycle. 2018;17(4):428-38.
62. Winkler IG, Sims NA, Pettit AR, Barbier V, Nowlan B, Helwani F, et al. Bone marrow macrophages maintain hematopoietic stem cell (HSC) niches and their depletion mobilizes HSCs. Blood. 2010;116(23):4815-28.
63. Seyfried AN, Maloney JM, MacNamara KC. Macrophages Orchestrate Hematopoietic Programs and Regulate HSC Function During Inflammatory Stress. Frontiers in Immunology. 2020;11.
64. Al-Matary YS, Botezatu L, Opalka B, Hönes JM, Lams RF, Thivakaran A, et al. Acute myeloid leukemia cells polarize macrophages towards a leukemia supporting state in a Growth factor independence 1 dependent manner. Haematologica. 2016;101(10):1216-27.
65. Yang X, Feng W, Wang R, Yang F, Wang L, Chen S, et al. Repolarizing heterogeneous leukemia-associated macrophages with more M1 characteristics eliminates their pro-leukemic effects. Oncoimmunology. 2018;7(4):e1412910.
66. Neering SJ, Bushnell T, Sozer S, Ashton J, Rossi RM, Wang P-Y, et al. Leukemia stem cells in a genetically defined murine model of blast-crisis CML. Blood. 2007;110(7):2578-85.
67. Li W, Li Y, Jin X, Liao Q, Chen Z, Peng H, et al. CD38: A Significant Regulator of Macrophage Function. Front Oncol. 2022;12:775649.
68. Chávez-Galán L, Olleros ML, Vesin D, Garcia I. Much More than M1 and M2 Macrophages, There are also CD169+ and TCR+ Macrophages. Frontiers in Immunology. 2015;6.
69. Mussai F, De Santo C, Abu-Dayyeh I, Booth S, Quek L, McEwen-Smith RM, et al. Acute myeloid leukemia creates an arginase-dependent immunosuppressive microenvironment. Blood. 2013;122(5):749-58.
70. Jablonski KA, Amici SA, Webb LM, Ruiz-Rosado JdD, Popovich PG, Partida-Sanchez S, et al. Novel Markers to Delineate Murine M1 and M2 Macrophages. PLOS ONE. 2015;10(12):e0145342.
71. Mao Z, Zhang J, Shi Y, Li W, Shi H, Ji R, et al. CXCL5 promotes gastric cancer metastasis by inducing epithelial-mesenchymal transition and activating neutrophils. Oncogenesis. 2020;9(7):63.
72. Kessenbrock K, Plaks V, Werb Z. Matrix metalloproteinases: regulators of the tumor microenvironment. Cell. 2010;141(1):52-67.

73. Bhattacharya A, Chowdhury A, Chaudhury K, Shukla PC. Proprotein convertase subtilisin/kexin type 9 (PCSK9): A potential multifaceted player in cancer. Biochim Biophys Acta Rev Cancer. 2021;1876(1):188581.
74. Moll NM, Ransohoff RM. CXCL12 and CXCR4 in bone marrow physiology. Expert Rev Hematol. 2010;3(3):315-22.
75. Kim M, Choi HY, Woo JW, Chung YR, Park SY. Role of CXCL10 in the progression of in situ to invasive carcinoma of the breast. Scientific Reports. 2021;11(1):18007.
76. Zhang Y, Lazarus J, Steele NG, Yan W, Lee H-J, Nwosu ZC, et al. Regulatory T-cell Depletion Alters the Tumor Microenvironment and Accelerates Pancreatic Carcinogenesis. Cancer Discovery. 2020;10(3):422-39.
77. Yeh SCA, Hou J, Wu JW, Yu S, Zhang Y, Belfield KD, et al. Quantification of bone marrow interstitial pH and calcium concentration by intravital ratiometric imaging. Nature Communications. 2022;13(1):393.
78. Stein M, Keshav S, Harris N, Gordon S. Interleukin 4 potently enhances murine macrophage mannose receptor activity: a marker of alternative immunologic macrophage activation. Journal of Experimental Medicine. 1992;176(1):287-92.
79. Doherty TM, Kastelein R, Menon S, Andrade S, Coffman RL. Modulation of murine macrophage function by IL-13. The Journal of Immunology. 1993;151(12):7151-60.
80. Doyle AG, Herbein G, Montaner LJ, Minty AJ, Caput D, Ferrara P, et al. Interleukin-13 alters the activation state of murine macrophages in vitro: Comparison with interleukin-4 and interferon-γ. European Journal of Immunology. 1994;24(6):1441-5.
81. Bailey JD, Diotallevi M, Nicol T, McNeill E, Shaw A, Chuaiphichai S, et al. Nitric Oxide Modulates Metabolic Remodeling in Inflammatory Macrophages through TCA Cycle Regulation and Itaconate Accumulation. Cell Reports. 2019;28(1):218-30.e7.
82. Ackun-Farmmer MA, Soto CA, Lesch ML, Byun D, Yang L, Calvi LM, et al. Reduction of leukemic burden via bone-targeted nanoparticle delivery of an inhibitor of C-chemokine (C-C motif) ligand 3 (CCL3) signaling. Faseb j. 2021;35(4):e21402.
83. Pinho S, Lacombe J, Hanoun M, Mizoguchi T, Bruns I, Kunisaki Y, et al. PDGFRα and CD51 mark human nestin+ sphere-forming mesenchymal stem cells capable of hematopoietic progenitor cell expansion. J Exp Med. 2013;210(7):1351-67.
84. Morikawa S, Mabuchi Y, Kubota Y, Nagai Y, Niibe K, Hiratsu E, et al. Prospective identification, isolation, and systemic transplantation of multipotent mesenchymal stem cells in murine bone marrow. J Exp Med. 2009;206(11):2483-96.
85. Frisch BJ, Hoffman CM, Latchney SE, LaMere MW, Myers J, Ashton J, et al. Aged marrow macrophages expand platelet-biased hematopoietic stem cells via interleukin-1B. JCI Insight. 2019;4(10).
86. Morrison BM, Tsingalia A, Vidensky S, Lee Y, Jin L, Farah MH, et al. Deficiency in monocarboxylate transporter 1 (MCT1) in mice delays regeneration of peripheral nerves following sciatic nerve crush. Exp Neurol. 2015;263:325-38.
87. Bisetto S, Whitaker-Menezes D, Wilski NA, Tuluc M, Curry J, Zhan T, et al. Monocarboxylate Transporter 4 (MCT4) Knockout Mice Have Attenuated 4NQO Induced Carcinogenesis; A Role for MCT4 in Driving Oral Squamous Cell Cancer. Front Oncol. 2018;8:324.

88. Benjamin D, Robay D, Hindupur SK, Pohlmann J, Colombi M, El-Shemerly MY, et al. Dual Inhibition of the Lactate Transporters MCT1 and MCT4 Is Synthetic Lethal with Metformin due to NAD+ Depletion in Cancer Cells. Cell Rep. 2018;25(11):3047-58.e4.
89. Sautchuk R, Eliseev RA. Cell energy metabolism and bone formation. Bone Reports. 2022;16:101594.
90. Bottomly D, Long N, Schultz AR, Kurtz SE, Tognon CE, Johnson K, et al. Integrative analysis of drug response and clinical outcome in acute myeloid leukemia. Cancer Cell. 2022;40(8):850-64.e9.
91. Jaynes JM, Sable R, Ronzetti M, Bautista W, Knotts Z, Abisoye-Ogunniyan A, et al. Mannose receptor (CD206) activation in tumor-associated macrophages enhances adaptive and innate antitumor immune responses. Science Translational Medicine. 2020;12(530):eaax6337.
92. Xu ZJ, Gu Y, Wang CZ, Jin Y, Wen XM, Ma JC, et al. The M2 macrophage marker CD206: a novel prognostic indicator for acute myeloid leukemia. Oncoimmunology. 2020;9(1):1683347.
93. Su X, Xu Y, Fox GC, Xiang J, Kwakwa KA, Davis JL, et al. Breast cancer-derived GM-CSF regulates arginase 1 in myeloid cells to promote an immunosuppressive microenvironment. J Clin Invest. 2021;131(20).
94. Wang J, Huang H, Lu J, Bi P, Wang F, Liu X, et al. Tumor cells induced-M2 macrophage favors accumulation of Treg in nasopharyngeal carcinoma. Int J Clin Exp Pathol. 2017;10(8):8389-401.
95. Sun W, Wei F-Q, Li W-J, Wei J-W, Zhong H, Wen Y-H, et al. A positive-feedback loop between tumour infiltrating activated Treg cells and type 2-skewed macrophages is essential for progression of laryngeal squamous cell carcinoma. British Journal of Cancer. 2017;117(11):1631-43.
96. Noy R, Pollard Jeffrey W. Tumor-Associated Macrophages: From Mechanisms to Therapy. Immunity. 2014;41(1):49-61.
97. Chen T, Zhou Y, Tan W-S. Influence of lactic acid on the proliferation, metabolism, and differentiation of rabbit mesenchymal stem cells. Cell Biology and Toxicology. 2009;25(6):573-86.
98. Wei L, Wei W, Qi Z, Yuanmei Z, Yun W, Haiyan L, et al. Small bone marrow adipocytes predict poor prognosis in acute myeloid leukemia. Haematologica. 2018;103(1):e21-e4.
99. Saulle E, Spinello I, Quaranta MT, Pasquini L, Pelosi E, Iorio E, et al. Targeting Lactate Metabolism by Inhibiting MCT1 or MCT4 Impairs Leukemic Cell Proliferation, Induces Two Different Related Death-Pathways and Increases Chemotherapeutic Sensitivity of Acute Myeloid Leukemia Cells. Frontiers in Oncology. 2021;10.
100. Man CH, Mercier FE, Liu N, Dong W, Stephanopoulos G, Jiang L, et al. Proton export alkalinizes intracellular pH and reprograms carbon metabolism to drive normal and malignant cell growth. Blood. 2022;139(4):502-22.
101. Ranganathan P, Shanmugam A, Swafford D, Suryawanshi A, Bhattacharjee P, Hussein MS, et al. GPR81, a Cell-Surface Receptor for Lactate, Regulates Intestinal Homeostasis and Protects Mice from Experimental Colitis. J Immunol. 2018;200(5):1781-9.
102. Ahmed K, Tunaru S, Tang C, Müller M, Gille A, Sassmann A, et al. An Autocrine Lactate Loop Mediates Insulin-Dependent Inhibition of Lipolysis through GPR81. Cell Metabolism. 2010;11(4):311-9.